Wissenschaftlich-Technische Berichte
FZR- 399
März 2004
ISSN 1437-322X

Susanne Sachs, Katja Schmeide, Vinzenz Brendler,
Adéla Křepelová, Jens Mibus, Gerhard Geipel,
Karl-Heinz Heise, Gert Bernhard

Investigation of the Complexation and the Migration of Actinides and Non-radioactive Substances with Humic Acids under Geogenic Conditions

Complexation of Humic Acids with Actinides in the Oxidation State IV Th, U, Np

Forschungszentrum Rossendorf
Mitglied der Leibniz-Gemeinschaft

Wissenschaftlich-Technische Berichte
FZR-399
März 2004

Susanne Sachs, Katja Schmeide, Vinzenz Brendler,
Adéla Křepelová, Jens Mibus, Gerhard Geipel,
Karl-Heinz Heise, Gert Bernhard

Investigation of the Complexation and the Migration of Actinides and Non-radioactive Substances with Humic Acids under Geogenic Conditions

Complexation of Humic Acids with Actinides in the Oxidation State IV Th, U, Np

Forschungszentrum
Rossendorf

Das diesem Bericht zugrundeliegende Vorhaben wurde mit Mitteln des Bundesministeriums für Wirtschaft und Arbeit unter dem Förderkennzeichen 02 E 9299 gefördert. Die Verantwortung für den Inhalt dieser Veröffentlichung liegt bei den Autoren.

Vorhaben:

UNTERSUCHUNGEN ÜBER DIE KOMPLEXIERUNG UND MIGRATION VON ACTINIDEN UND NICHTRADIOAKTIVEN STOFFEN MIT HUMINSÄUREN UNTER GEOGENEN BEDINGUNGEN

KOMPLEXIERUNG VON HUMINSÄUREN MIT ACTINIDEN IN DER OXIDATIONSSTUFE IV Th, U, Np

Abstract

Objective of this project was the study of basic interaction and migration processes of actinides in the environment in presence of humic acids (HA). To obtain more basic knowledge on these interaction processes synthetic HA with specific functional properties as well as ^{14}C-labeled HA were synthesized and applied in comparison to the natural HA Aldrich. One focus of the work was on the synthesis of HA with distinct redox functionalities. The obtained synthetic products that are characterized by significantly higher Fe(III) redox capacities than Aldrich HA were applied to study the redox properties of HA and the redox stability of U(VI) humate complexes. It was confirmed that phenolic OH groups play an important role for the redox properties of HA. However, the results indicate that there are also other processes than the single oxidation of phenolic OH groups and/or other functional groups contributing to the redox behavior of HA. A first direct-spectroscopic proof for the reduction of U(VI) by synthetic HA with distinct redox functionality was obtained.
The complexation behavior of synthetic and natural HA with actinides (Th, Np, Pu) was studied. Structural parameters of Pu(III), Th(IV), Np(IV) and Np(V) humates were determined by X-ray absorption spectroscopy (XAS). The results show that carboxylate groups dominate the interaction between HA and actinide ions. These are predominant monodentately bound. The influence of phenolic OH groups on the Np(V) complexation by HA was studied with modified HA (blocked phenolic OH groups). The blocking of phenolic OH groups induces a decrease of the number of maximal available complexing sites of HA, whereas complex stability constant and Np(V) near-neighbor surrounding are not affected.
The effects of HA on the sorption and migration behavior of actinides was studied in batch and column experiments. Th(IV) sorption onto quartz and Np(V) sorption onto granite and its mineral constituents are affected by the pH value and the presence of HA. HA exhibits a significant influence on the transport of U(IV) and U(VI) in a laboratory quartz sand system.
In order to provide the basis for a more reliable modeling of the actinide transport, the metal ion complexation with HA has to be integrated into existing geochemical speciation codes. Within this project the metal ion charge neutralization model was embedded into the geochemical modeling code EQ3/6. In addition to that, a digital data base was developed which covers HA complexation data basing on the charge neutralization model.

Zusammenfassung

Ziel des Projektes war die Untersuchung grundlegender Wechselwirkungs- und Migrationsprozesse von Actiniden in der Umwelt in Gegenwart von Huminsäuren (HS). Zur Erzielung grundlegenden Wissens über diese Prozesse wurden synthetische HS mit spezifischen funktionellen Eigenschaften sowie ^{14}C-markierte HS synthetisiert und im Vergleich zur natürlichen HS Aldrich eingesetzt. Ein Schwerpunkt der Arbeiten lag auf der Synthese von HS mit ausgeprägter Redoxfunktionalität. Die synthetisierten Produkte, die durch signifikant größere Fe(III)-Redoxkapazitäten als Aldrich HS charakterisiert sind, wurden zur Untersuchung der Redoxeigenschaften von HS und der Redoxstabilität von U(VI)-Humat-Komplexen eingesetzt. Es wurde bestätigt, dass phenolische OH-Gruppen eine wichtige Rolle für das Redoxverhalten von HS spielen. Weitere Prozesse als die einfache Phenoloxidation und/oder andere funktionelle Gruppen tragen jedoch zum Redoxverhalten von HS bei. Ein erster direkt-spektroskopischer Nachweis für die Reduktion von U(VI) durch ausgeprägt reduzierende HS wurde erbracht.
Das Komplexbildungsverhalten synthetischer und natürlicher HS mit Actiniden (Th, Np, Pu) wurde untersucht. Mittels Röntgenabsorptionsspektroskopie (XAS) wurden Strukturparameter für Pu(III)-, Th(IV)-, Np(IV)- und Np(V)-Humate bestimmt. Die Ergebnisse zeigen, dass vorwiegend monodentat koordinierte Carboxylgruppen die Wechselwirkung zwischen HS und Actiniden dominieren. Der Einfluss phenolischer OH-Gruppen auf die Np(V)-HS-Komplexierung wurde mit modifizierten HS (blockierte phenolische OH-Gruppen) untersucht. Die Blockierung phenolischer OH-Gruppen bewirkt eine Verringerung der Anzahl an verfügbaren Bindungsplätzen der HS. Dagegen bleiben Stabilitätskonstante und Np(V)-Nahordnung davon unbeeinflusst.
Der Einfluss von HS auf das Sorptions- und Migrationsverhalten von Actiniden wurde in Batch- und Säulenversuchen untersucht. Th(IV)-Sorption an Quarz sowie Np(V)-Sorption an Granit und seinen mineralischen Bestandteilen werden durch pH-Wert und HS beeinflusst. HS zeigen einen signifikanten Einfluss auf den Transport von U(IV) und U(VI) in Quarzsand auf Labormaßstab.
Zur zuverlässigen Modellierung des Actiniden-Transports ist die Integration der Metallionen-HS-Komplexierung in geochemische Speziationscodes erforderlich. Dazu wurde das Metallionen-Ladungsneutralisationsmodell in den geochemischen Modellierungscode EQ3/6 implementiert. Darüber hinaus wurde eine digitale Datenbank entwickelt, die auf dem Ladungsneutralisationsmodell basierende HS-Komplexierungsdaten enthält.

Content

1 Introduction

Studies on the migration behavior of radioactive and non-radioactive toxic substances are of high importance for the reliable long-term risk assessment of potential underground nuclear waste repositories, of facilities of the former uranium mining and milling sites in Saxony and Thuringia (Germany), and of subsurface dumps and sites with radioactive and/or heavy metal containing inventory. Depending on the prevailing geochemical conditions different materials and processes can influence the behavior of such pollutants in natural aquifer systems. Therefore, knowledge on these processes and materials is indispensable for the trustworthy modeling of the migration of radioactive and toxic metal ions, e.g., actinide ions, in the nature.
Besides inorganic ligands such as sulfate, phosphate, arsenate and silicate, humic acids (HA), organic macromolecules ubiquitous found in natural environments, play an important role in the interaction processes of actinide ions. HA are soluble in the pH range of natural waters and possess the ability for complex and colloid formation. In addition to that, HA are characterized by redox properties, which can influence the oxidation state of metal ions. For instance, HA can reduce Np(VI) to Np(V), Pu(VI) to Pu(IV) [1] and U(VI) to U(IV) [2]. Due to these properties HA can affect the speciation of metal ions, e.g., actinide ions, and therefore, their migration in the environment. The colloidal behavior of HA together with their high complexing ability for metal ions may cause an effective transport mechanism for actinides.
The chemistry of penta- and hexavalent actinides under aerobic conditions was already subject of a number of investigations also in the presence of HA. However, under reducing conditions, as prevalent in deep underground environments, e.g., in deep groundwaters [3], actinides can occur in the tetravalent oxidation state, which then dominates their speciation and migration. The data base for the interaction behavior of actinides in the tetravalent oxidation state is small and the basic scientific understanding of these processes is low. The existing data on the interaction between HA and tetravalent actinides (e.g., [4-9]) is not sufficient for the geochemical modeling of the migration behavior of actinides.

The main focus of this research project was on the study of basic interaction and migration processes of actinides (U, Np, Pu, Th) in different oxidation states, especially in the tetravalent, in the presence of HA. In order to gain a more basic knowledge on these processes, synthetic HA with different functional properties and ^{14}C-labeled HA were applied in comparison to natural HA from Aldrich. Partially, these substances were already developed and successfully used in our previous project funded by BMBF (contract number 02 E 88150), where the

interaction between HA and uranium under aerobic conditions was the main subject of interest [10]. Within the present project new batches of HA were prepared and synthesis methods were optimized. In addition to that, synthetic HA with distinct redox functionalities were developed for detailed studies on the redox properties of HA and on the redox stability of actinide humate complexes. In order to improve the knowledge on the complexation between HA and actinides in lower oxidation states and for the enhancement of existing complexation models for the HA complexation, thermodynamic and structural studies on actinide (Pu(III), Np(IV), Np(V), Th(IV)) humate complexes were performed. The influence of HA on the sorption and migration behavior of actinides (U(IV), U(VI), Th(IV), Np(V)) was studied in batch and column experiments, respectively. The reliable geochemical modeling of the actinide transport requires the integration of the actinide HA complexation as well as of current experimental data into existing modeling programs. It was the aim of this project to integrate the HA metal ion complexation in a suitable modeling code. In addition to that, it was focused on the development of a digital data base on the HA metal ion complexation because no accepted and consistent data base is available for that up to now.

The research project was performed in close collaboration with the R&D projects of the Universities of Mainz and Saarbrücken and of the Institute for Interdisciplinary Isotope Research Leipzig (IIF) that were funded by the Bundesministerium für Wirtschaft und Arbeit (BMWA) under contract number 02 E 9309 and 02 E 9329, respectively, and with the Institute for Nuclear Waste Management (INE) of the Forschungszentrum Karlsruhe.

Within the framework of this project the main emphasis of the studies of the Institute of Radiochemistry (Forschungszentrum Rossendorf) was on the following topics:

1. Synthesis and characterization of HA model substances with different functionalities including their modification and ^{14}C-labeling. Synthetic HA were to be provided to the project partners. Development of synthetic HA with distinct redox functionalities.
2. Studies on the redox properties of HA and on the redox stability of actinide humate complexes.
3. Structural and thermodynamical studies on the actinide complexation by HA applying synthetic HA model substances and natural HA. The main focus was on structural studies on the interaction of HA with actinides in lower oxidation states (Th, Np, Pu) and on the influence of phenolic OH groups on the Np(V) complexation by HA.

4. Studies on the influence of HA on the sorption of Np(V), Th(IV) onto relevant rock materials and minerals and on the migration of U(IV)/U(VI) in a laboratory system.
5. Software and model development: Integration of the metal ion charge neutralization model [11] for the description of the HA complexation into the speciation code EQ3/6 [12].
6. Development of a digital data base for the HA complexation based on the metal ion charge neutralization model.

The scientific results of this project are described in detail in the following sections.

2 Natural humic acid reference material

As in the previous project [10], commercially available natural HA from Aldrich (AHA; Aldrich, Steinheim, Germany) was used as reference material. Before use, the sodium salt of AHA (Batch H1, 675-2) was purified according to the purification method described by Kim and Buckau [13] in order to remove inorganic contaminants of this substance.
For preparation of batch A2/98, the sodium salt of AHA was dissolved in 0.1 M NaOH (Merck, Darmstadt, Germany) containing 0.01 M NaF. The solution was stirred over night under nitrogen atmosphere. After that, the solution was centrifuged to separate the alkali-insoluble components of the sodium humate. To precipitate the HA, the supernatant was acidified with HCl (Merck) to pH 1. The HA precipitate was isolated by centrifugation and washed with 0.1 M HCl and water. The whole purification procedure was repeated three times. Subsequently, purified HA AHA (batch A2/98) was dried by lyophilization.

3 Synthesis and characterization of humic acids with specific functional properties

In order to improve the knowledge on the interaction processes between HA and metal ions, e.g., actinide ions, various HA model substances with different functional properties were already developed at the Institute of Radiochemistry. These include synthetic HA with different functional group contents and various structural elements [10,14], chemically modified HA with blocked phenolic OH groups [10,15,16] as well as ^{14}C-labeled HA [10,17]. Within this project, synthetic HA with distinct redox functionalities were developed.

The following paragraphs show the synthesis, modification, ^{14}C-labeling and characterization of different synthetic HA model substances with various functional properties that were performed within the scope of this project.

3.1 Synthesis and ^{14}C-labeling of humic acid type M42

3.1.1 Synthesis of humic acid type M42

Within this project a new batch of synthetic HA type M42 (batch M145) was synthesized. It was made available to all project partners for comparative studies.

The basic synthesis of HA type M42 was already described in detail in [10]. It starts from a mixture of 22 g glutamic acid monohydrate (Merck), 33 g xylose (Merck) and 60 mL water which is heated for 92 hours at 80 ± 2 °C under reflux and inert gas. After expiration of the reaction time and cooling of the reaction mixture the formed solid melanoidin fraction is separated from the liquid fraction by centrifugation. Then, the solid product is washed and ground with ethanol (Merck) and ether (Merck). Similar to the isolation of natural HA [18], the HA-like melanoidin fractions are extracted by stirring the solid product with 2 M NaOH (Merck) for 8 hours under inert gas. The synthetic HA is precipitated from the alkaline solution with 2 M HCl (Merck). The resulting HA precipitate is washed, dialyzed using dialysis tubes (Spectra/Por®, exclusion limit MWCO <1000, Roth, Karlsruhe, Germany) against purified water, and lyophilized.

52 g synthetic HA type M42 (batch M145) were synthesized. For that, seven synthesis sequences, each with six parallel batches, were performed.

3.1.2 Synthesis of ^{14}C-labeled humic acid type M42 ([^{14}C]M42)

Carbon-14 labeled synthetic HA are synthesized according to the unlabeled HA type M42, however, applying ^{14}C-labeled amino acids, e.g., [u-^{14}C]glutamic acid, as starting materials [10,17]. In the present project two batches of ^{14}C-labeled synthetic HA type M42 ([^{14}C]M42) were synthesized as described above, batch M170 and M180. Batch M170 was synthesized starting from 27.75 g xylose, 18.33 g glutamic acid monohydrate and 50 mL water. 2 mg [u-^{14}C]glutamic acid (111 MBq) were added to the precursor substances. Batch M180 was prepared from 8.95 g xylose, 5.91 g glutamic acid monohydrate, 5.4 mg [u-^{14}C]glutamic acid

(296 MBq) and 16 mL water. These syntheses resulted in 932 mg (batch M170) and 368 mg (batch M180) synthetic HA type [^{14}C]M42 with specific activities of 2.38 MBq/g and 17.0 MBq/g, respectively. In both syntheses, only 2 % of the starting ^{14}C-activity were incorporated into the HA-like synthetic product. Evaluating this radiochemical yield is has to be taken into account that the HA-like fraction of the reaction product is small compared to the other fractions that are formed during the synthesis, e.g., preliminary products, humin and fulvic acid-like fractions. The differences in the specific activities of the reaction product are due to the different specific activities of the reaction mixtures used for the syntheses.
100 mg of synthetic HA type [^{14}C]M42 (batch M180) were provided to the Institute of Interdisciplinary Isotope Research Leipzig for sorption experiments.

3.1.3 Characterization of synthetic humic acid type M42 and [^{14}C]M42

Table 3.1 summarizes the elemental compositions and the functional group contents of the newly synthesized batches of HA type M42 and [^{14}C]M42 in comparison to the data of the purified, commercially available, natural HA from Aldrich (AHA) and natural HA from literature [19,20].
Synthetic HA type M42 shows an elemental composition that is similar to those of AHA and other natural HA. It contains no sulfur due to the use of sulfur-free precursor substances. Comparing the ash content of synthetic HA type M42 with that of AHA it becomes obvious that the synthetic product is characterized by a very low content on inorganic constituents.
The carboxyl group content and the proton exchange capacity (PEC) of HA type M42 are comparable to those of AHA and other naturally occurring HA. In addition to that, HA type M42 shows an amount of phenolic/acidic OH groups that is similar to natural HA. Comparing the functional group contents of the unlabeled and ^{14}C-labeled synthetic HA type M42 it becomes obvious that these agree well in the range of their standard deviations. This fact points to a good reproducibility of the synthesis with regard to the HA functional group content.

Tab. 3.1: Characterization of HA type M42 (batch M145) and [^{14}C]M42 (batch M170 and M180) in comparison to natural HA.

HA	Elemental composition						
	C (%)	H [a] (%)	N (%)	S (%)	O [b] (%)	Ash (%)	Moisture (%)
Type M42 (batch M145)	56.1 ± 0.3	4.1 ± 0.1	4.4 ± 0.1	-	26.8 ± 0.3	0.11	8.4
AHA (batch A2/98)	58.6 ± 0.1	3.0 ± 0.1	0.8 ± 0.1	3.8 ± 0.1	23.5 ± 0.1	2.39	7.9
Natural [19]	50 - 60	4 – 6	2 - 6	0 - 2	30 – 35		

	Functional groups		
	COOH [c] (meq/g)	PEC [d] (meq/g)	Phenolic/acidic OH [e] (meq/g)
Type M42 (batch M145)	3.76 ± 0.09	3.51 ± 0.07	2.0 ± 0.2
Type [^{14}C]M42 (batch M170)	3.63 ± 0.03	3.55 ± 0.05	Not measured
Type [^{14}C]M42 (batch M180)	3.59 ± 0.01	3.36 ± 0.53	Not measured
AHA (batch A2/98)	4.49 ± 0.14	4.60 ± 0.08	3.1 ± 0.1
Natural [20]	1.5 – 5.7		2.1 – 5.7

[a] Corrected for the water content of the HA. [b] The oxygen content was calculated from the difference to 100 % in consideration of the ash and moisture content of the HA. [c] Determined by calcium acetate exchange [21]. [d] PEC: Proton Exchange Capacity. Determined by potentiometric titration. [e] Radiometrically determined [10,22].

In Fig. 3.1 the FTIR spectra (FTIR spectrometer Spectrum 2000, Perkin Elmer; KBr method) of HA type M42 and [^{14}C]M42 are depicted in comparison to that of natural HA from Aldrich. In general, synthetic HA type M42 shows IR absorption bands which are similar to those observed for natural HA [10,19]. The comparison of the FTIR spectra of HA type M42 and [^{14}C]M42 in terms of the position of the IR absorption bands and the band intensities shows that all three spectra are nearly identical. Thus, it can be concluded that the unlabeled and ^{14}C-labeled synthetic HA type M42 show comparable structures, which points to a good reproducibility of the synthesis concerning the HA structure.

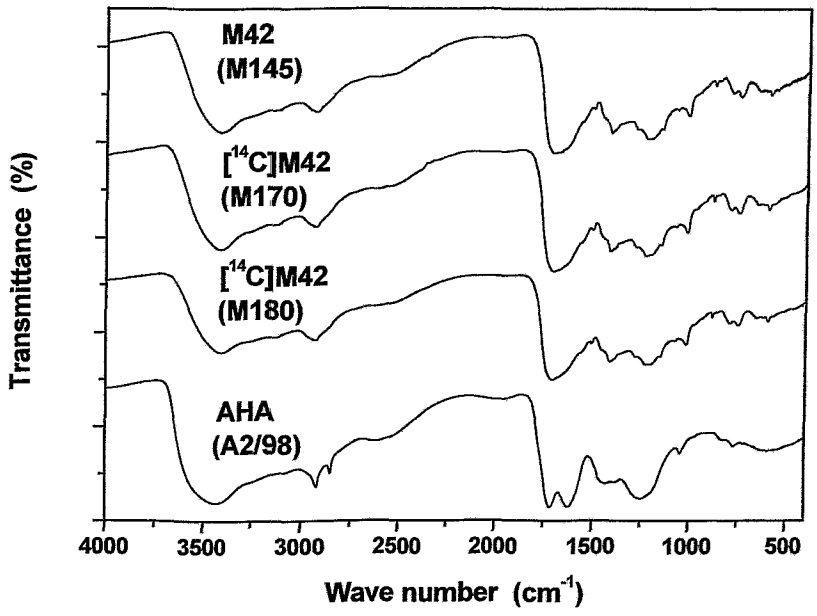

Fig. 3.1: FTIR spectra of unlabeled and ^{14}C-labeled synthetic HA type M42 in comparison to natural HA AHA.

3.2 Synthesis and characterization of chemically modified humic acids with blocked phenolic OH groups

In order to study the influence of phenolic OH groups on the interaction behavior of HA we developed and verified a method for the synthesis of chemically modified HA with blocked phenolic OH groups by methylation with diazomethane [10,15,16]. Such modified HA were already successfully used to study the influence of phenolic OH groups on the U(VI) complexation by natural and synthetic HA [15,23].

Figure 3.2 shows the reaction scheme for the chemical modification process applied. In the first modification step the original HA is methylated with diazomethane for three hours at –5 to 5 °C in methanolic solution. This methylation results in the formation of methyl esters of carboxyl groups and methyl ethers of phenolic/acidic OH groups. The methylation is repeated several times and stopped when the incorporation of diazomethane into the HA molecule is completed. The solvent, that is distilled from the reaction mixture, shows then the yellow color of the non-reacted excess of diazomethane. In the second modification step the methylated HA is treated with alkaline solution (2 M NaOH) at room temperature under inert gas to hydrolyze the methyl esters of carboxyl groups that were formed by methylation with diazo-

methane. However, methyl ether groups of phenolic OH groups remain blocked because these cannot be decomposed by alkaline hydrolysis. After hydrolysis, the modified HA with blocked phenolic OH groups is precipitated with 2 M HCl, separated by centrifugation, dialyzed (MWCO < 1000), and lyophilized. It should be noted that in addition to phenolic OH groups also other acidic OH groups of the HA, i.e., enolic OH groups or acidic OH groups substituted to five-membered heterocycles can be methylated with diazomethane, resulting in non-hydrolizable ether groups. Applying this method we obtained partially modifications of HA phenolic/acidic OH groups. We modified for instance, 68 % and 74 % of the originally occurring phenolic/acidic OH groups of HA AHA and M42, respectively [10].

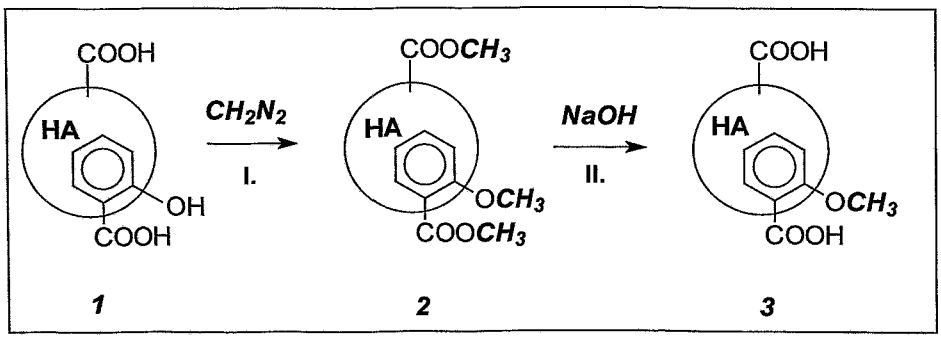

Fig. 3.2: Scheme for the synthesis of chemically modified HA with blocked phenolic OH groups. 1: original HA, 2: methylated HA (type HA-B), 3: HA with blocked phenolic OH groups (type HA-PB).

In the present project the modification procedure that was applied up to now was optimized. In order to achieve a complete blocking of all phenolic/acidic OH groups of HA type M42 and AHA the whole modification procedure (step 1: methylation with diazomethane, step 2: alkaline hydrolysis of the methylated HA) was repeated three times. That means, the methylated HA with blocked phenolic/acidic OH groups that was obtained within the first modification cycle was subjected to a second and third methylation cycle.

Table 3.2 shows the functional group contents of modified HA type M42 (M42-PB) and AHA (AHA-PB) that were obtained with the optimized methylation procedure in comparison to those of the unmodified HA. After three methylation cycles 75 % and 84 % of the initially occurring phenolic/acidic OH groups of HA type M42 and AHA, respectively, were modified. These results show that even after a threefold replication of the methylation procedure a complete blocking of all phenolic/acidic OH groups is not possible.

Tab. 3.2: Functional group contents of modified and unmodified HA type M42 and AHA.

HA	COOH [a] (meq/g)	PEC [b] (meq/g)	Phenolic/acidic OH [c] (meq/g)	Phenolic/acidic OH : COOH
Type M42 (batch M145)	3.76 ± 0.09	3.51 ± 0.07	2.0 ± 0.2	0.53
M42-PB (batch M171)	3.12 ± 0.07	3.23 ± 0.15	0.5	0.16
AHA (batch A2/98)	4.49 ± 0.14	4.60 ± 0.08	3.1 ± 0.1	0.69
AHA-PB (batch M173)	2.67 ± 0.01	3.13 ± 0.15	0.5	0.19

[a] Determined by calcium acetate exchange [21]. [b] PEC: Proton Exchange Capacity. Determined by potentiometric titration. [c] Radiometrically determined [10,22].

Up to now, it could not be confirmed whether those functional groups that are determined after the modification are unmodified original phenolic/acidic OH groups of the HA or acidic OH groups that were released during the derivatization process by uncovering formerly sterically hindered functional groups. Comparing the carboxyl group content and the PEC of the corresponding unmodified and modified HA it becomes obvious that the modified HA, especially HA AHA, have less carboxyl groups and lower PEC than the original unmodified HA. An incomplete hydrolysis of methyl ester groups that were formed during the methylation could be one possible reason for that observation. ^{13}C-CP/MAS-NMR spectroscopic results support this conclusion [16]. Nevertheless, for both HA the molar ratio of phenolic/acidic OH to carboxyl groups becomes smaller due to the modification. This enables us to use these chemically modified HA to study the impact of phenolic/acidic OH groups on the interaction between HA and metal ions.

3.3 Humic acids with distinct redox functionalities

The migration behavior of toxic and radiotoxic metal ions, e.g., actinides, strongly depends on their oxidation state that can be influenced by HA [1]. Therefore, the detailed description of the influence of HA on the mobility of actinides in the environment requires the understanding of the effects of HA on the oxidation states of actinides besides the knowledge on the actinide ion complexation by HA. In order to study the redox properties of HA and the redox stability of actinide humate complexes in more detail, we developed synthetic HA model substances with pronounced redox functionalities.

3.3.1 Synthesis of humic acid-like oxidation products from phenolic compounds

The redox activity of humic substances can be ascribed to the redox system hydroquinone-quinone and the oxidation of phenolic OH groups to phenoxy radicals [24] with their typical subsequent reactions, such as coupling reactions and tautomerizations. Both systems are schematically shown in Fig. 3.3 [25]. Based on this knowledge, we decided to synthesize HA with high amounts of phenolic OH groups in order to obtain HA with distinct redox functionalities.

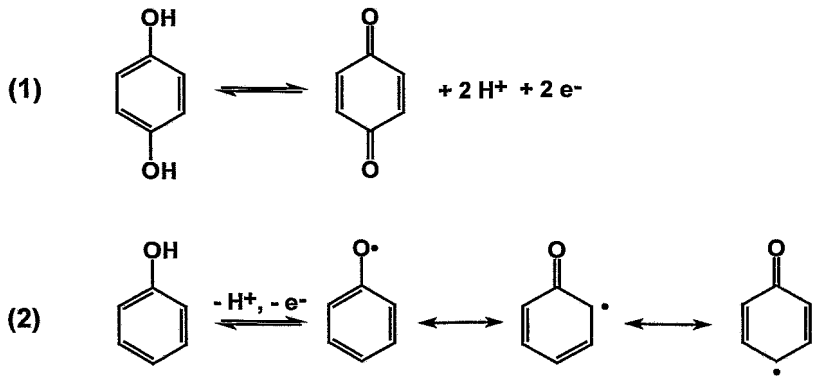

Fig. 3.3: Scheme for the redox system hydroquinone-quinone (1) and the oxidation of phenols to phenoxy radicals (2).

The performed syntheses are based on the oxidation of different phenolic compounds in alkaline solution in the absence or presence of amino acids. Potassium peroxodisulfate was used as oxidizing agent [26,27]. Within the project different types of HA-like oxidation products of phenolic compounds were synthesized starting from hydroquinone, catechol or vanillic acid in the absence or presence of glycine or glutamic acid. Table 3.3 summarizes the starting materials for the synthesized HA model substances.

Tab. 3.3: Starting materials for the synthesis of HA based on the oxidation of phenolic compounds (basic batch sizes).

HA	Phenolic compound		Amino acid	
Type Hyd	11.35 mmol	Hydroquinone	-	-
Type Hyd-Gly	11.35 mmol	Hydroquinone	11.35 mmol	Glycine
Type Hyd-Glu	11.35 mmol	Hydroquinone	5.69 mmol	Glutamic acid
Type Cat-Gly	11.35 mmol	Catechol	11.35 mmol	Glycine
Type Van-Gly	11.30 mmol	Vanillic acid	11.35 mmol	Glycine

For syntheses, the starting materials were dissolved in 0.1 M NaOH (425 mL for HA type Hyd and 450 mL for the other HA per basic batch size) at room temperature. Within one hour potassium peroxodisulfate (6.25 g per basic batch size) was charged to the reaction mixture at room temperature (HA type Hyd) or at 60 °C (HA type Hyd-Gly, Hyd-Glu, Cat-Gly, Van-Gly). After that, the reaction mixtures were cooled down and the HA-like fractions of the oxidation products were precipitated by addition of HCl. The HA precipitates were separated by centrifugation, purified by dialysis against purified water (MWCO <1000), and lyophilized.

3.3.2 Characterization of humic acid-like oxidation products from hydroquinone, catechol and vanillic acid

The HA-like oxidation products from phenolic compounds were characterized in terms of their elemental composition, functional group content and structure. In order to characterize the redox properties of these synthetic products we determined their Fe(III) redox capacities in comparison to HA type M42 and AHA. The Fe(III) redox capacity represents the charge equivalents per mass unit HA that can be transferred to Fe(III).

Elemental composition

The elemental compositions of the different oxidation products from phenolic compounds are summarized in Tab. 3.4 in comparison to those of HA type M42, AHA and natural HA from literature [19].

All synthetic products exhibit elemental compositions that are close to those of natural HA. Those oxidation products that were synthesized in the presence of glycine or glutamic acid are characterized by higher nitrogen contents compared to that of AHA due to the use of the nitrogen-containing starting materials. In comparison to synthetic HA type M42 (synthesis product of xylose and glutamic acid, cf. 3.1), the oxidation products from hydroquinone and catechol show lower hydrogen contents. This result points to a higher aromaticity of these substances due to their aromatic precursor substances.

Tab. 3.4: Elemental composition of HA-like oxidation products of phenolic compounds in comparsion to HA type M42 and natural HA.

HA	C (%)	H [a] (%)	N (%)	S (%)	O [b] (%)	Ash (%)	Moisture (%)
Type Hyd (batch R9/01)	59.8 ± 0.4	3.2 ± 0.1[c]	0.3 ± 0.1	0.3 ± 0.1	36.4 ± 0.4	n.m.[d]	n.m.
Type Hyd-Gly (batch R12/02)	54.2 ± 0.2	2.3 ± 0.2	5.3 ± 0.1	0.4 ± 0.1	26.7 ± 0.2	1.3	9.9
Type Hyd-Glu (batch R13/02)	53.7 ± 0.1	2.3 ± 0.1	2.0 ± 0.1	0.2 ± 0.1	28.2 ± 0.1	1.6	11.9
Type Cat-Gly (batch R18/02)	48.8 ± 0.1	2.8 ± 0.2	5.1 ± 0.1	0.9 ± 0.1	31.1 ± 0.2	1.7	9.5
Type Van-Gly (batch R5/02)	52.5 ± 0.5	4.0 ± 0.1[c]	4.5 ± 0.1	1.0 ± 0.3	38.0 ± 0.2	n.m.	n.m.
Type M42 (batch M145)	56.1 ± 0.3	4.1 ± 0.1	4.4 ± 0.1	-	26.8 ± 0.3	0.1	8.4
AHA (batch A2/98)	58.6 ± 0.1	3.0 ± 0.1	0.8 ± 0.1	3.8 ± 0.1	23.5 ± 0.1	2.4	7.9
Natural [19]	50 – 60	4 – 6	2 – 6	0 – 2	30 – 35		

[a] Corrected for the water content of the HA. [b] The oxygen content was calculated from the difference to 100 % in consideration of the ash and moisture content of the HA. [c] Not corrected for the water content of the HA. [d] n.m.: not measured.

Functional groups

Table 3.5 summarizes the functional group contents of the oxidation products from hydroquinone, catechol and vanillic acid in comparison to those of HA type M42 and natural HA. From this table it can be concluded that all HA-like oxidation products from diphenolic compounds (hydroquinone and catechol) show significantly higher phenolic/acidic OH group contents than HA type M42 and AHA. As expected, HA type Hyd shows the lowest carboxyl group content, but the highest amount on phenolic/acidic OH groups. In contrast to that, HA type Hyd-Gly, Hyd-Glu, Cat-Gly and Van-Gly, that were synthesized in the presence of amino acids show higher carboxyl group contents and PEC values. These are similar to those of HA type M42, AHA and other natural HA. Comparing the functional group contents of the oxidation products that were synthesized from different phenolic precursor substances (Hyd-Gly, Cat-Gly, Van-Gly) in the presence of glycine it becomes obvious that the synthetic product of vanillic acid and glycine (Van-Gly) shows the highest carboxyl group content but the lowest phenolic/acidic OH group as expected. Its amount on phenolic/acidic OH groups is comparable to that of AHA.

Tab. 3.5: Functional group contents of the HA-like oxidation products of phenolic compounds in comparison to HA type M42 and natural HA.

HA	COOH [a] (meq/g)	PEC [b] (meq/g)	Phenolic/acidic OH [c] (meq/g)
Hyd (batch R9/01)	1.92 ± 0.05	2.68 ± 0.01	7.2 ± 0.1
Hyd-Gly (batch R12/02)	4.30 ± 0.14	4.29 ± 0.13	5.3 ± 0.7
Hyd-Glu (batch R13/02)	3.84 ± 0.27	3.65 ± 0.14	5.8 ± 0.2
Cat-Gly (batch R18/02)	4.16 ± 0.04	3.59 ± 0.01	6.6 ± 0.7
Van-Gly (batch R5/02)	5.74 ± 0.08	5.17 ± 0.33	3.3 ± 1.3
M42 (batch M145)	3.76 ± 0.09	3.51 ± 0.07	2.0 ± 0.2
AHA (batch A2/98)	4.49 ± 0.14	4.60 ± 0.08	3.1 ± 0.1
Natural [20]	1.5 – 5.7		2.1 – 5.7

[a] Determined by calcium acetate exchange [21]. [b] PEC: Proton Exchange Capacity. Determined by potentiometric titration. [c] Radiometrically determined [10,22].

From these results it can be concluded that it is possible to vary the functionality of HA-like oxidation products from phenolic compounds by varying their precursor substances. A comparable conclusion was already drawn for the synthesis of HA model substances based on the melanoidin concept by condensation of reducing sugars and α-amino acids [14].

Structure

All synthetic HA were characterized by FTIR spectroscopy. By these measurements it was found that the oxidation products of phenolic compounds show FTIR absorption bands that are also characteristic for natural HA [10,19]. As expected, the synthetic products show variations in their structural elements due to the use of different precursor substances.

As example, Fig. 3.4 shows the FTIR spectra of the oxidation products from hydroquinone that were synthesized in the absence or presence of glycine and glutamic acid, respectively. The spectra are compared to that of HA AHA.

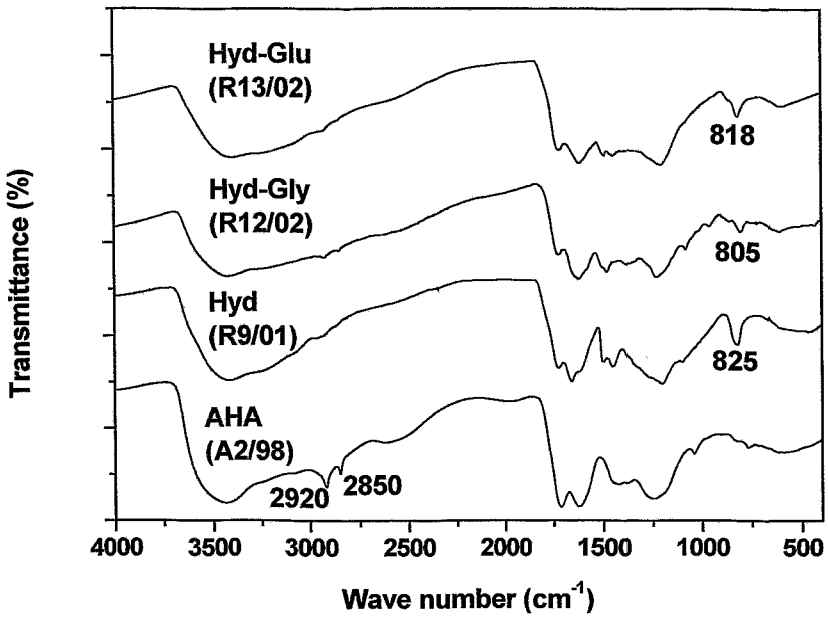

Fig. 3.4: FTIR spectra of HA-like oxidation products from hydroquinone in comparison to natural HA AHA.

In comparison to AHA all hydroquinone-based synthetic products show an intense absorption signal between 805 and 825 cm^{-1}. These bands are characteristic for para–substituted aromatic structural elements due to the use of hydroquinone as starting material. In addition to that, there are no significant FTIR bands indicating high amounts on aliphatic structural elements, as found for AHA at 2850 and 2920 cm^{-1}. From that it can be concluded that these synthetic products show a higher aromaticity than AHA. In all spectra FTIR absorption bands are found that confirm the occurrence of carboxyl groups in the HA structure (~1720 cm^{-1}).

Determination of Fe(III) redox capacities

According to Mack et al. [28,29] we determined for the synthetic HA the Fe(III) redox capacities in comparison to HA type M42 and AHA at pH 3. For that, suspensions of $FeCl_3$ and HA were shaken under nitrogen atmosphere and exclusion of light ([$FeCl_3$]: 8.2-8.5 mmol/L, [HA]: 0.12 g/L, pH 3, I: 0.1 M KCl). The Fe(II) ions formed by the reduction process depending on time were quantified in aliquots of the suspensions. Fe(II) was measured in form of the 1,10-phenanthroline complex by UV-vis spectroscopy (mod. 8452, Hewlett Packard) [30]. Prior to the quantification of Fe(II), the HA were separated by precipitation with H_2SO_4 and Fe(III) was masked by NH_4F. Besides the separation of HA from the sample aliquots, the ad-

dition of H_2SO_4 causes also the release of Fe(II) ions complexed with and/or sorbed onto HA molecules.

Furthermore, we determined for selected HA the Fe(III) redox capacities at pH 9.2 as described by Matthiessen [31]. For this we investigated solutions of $K_3[Fe(CN)_6]$ and HA under nitrogen atmosphere and exclusion of light ([$K_3[Fe(CN)_6]$]: 0.5 mmol/L, [HA]: 5 mg/L, I: 0.1 M KCl, borate buffer: pH 9.2). The time-dependent consumption of $K_3[Fe(CN)_6]$ due to the reduction of Fe(III) was followed by UV-vis spectroscopy.

The Fe(III) redox capacities of the HA depending on time were calculated from the measured Fe(II) concentrations in the HA suspensions with $FeCl_3$ and from the decrease of the $K_3[Fe(CN)_6]$ concentration in the solutions with HA.

Fe(III) redox capacities at pH 3

In Fig. 3.5 the Fe(III) redox capacities of the hydroquinone-based oxidation products are displayed in dependence on the reaction time. They are compared to those of HA type M42 and AHA.

In the initial phase of the reaction between HA and $FeCl_3$ the redox capacities increase fast with increasing reaction time. Then, a slower increase of the redox capacities was observed. This pH- and time-dependent Fe(III) reduction by HA was kinetically studied by Mack [29]. It was described by a fast and a subsequent slow kinetically controlled process.

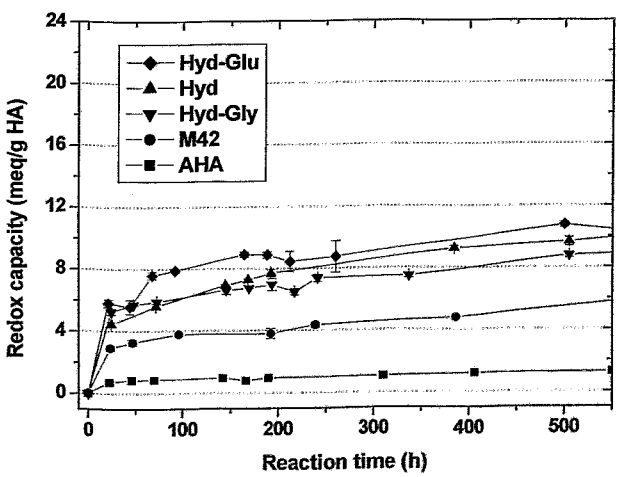

Fig. 3.5: Fe(III) redox capacities of hydroquinone-based HA-like oxidation products in comparison to HA AHA and M42.

From Fig. 3.5 it can be concluded that all synthetic HA based on hydroquinone show significantly higher Fe(III) redox capacities than HA type M42 and AHA. These higher redox capacities can be ascribed to the higher phenolic/acidic OH group contents of the oxidation products from hydroquinone. Similar results were found comparing the data of the oxidation products from different phenolic compounds and glycine which are depicted in Fig. 3.6.

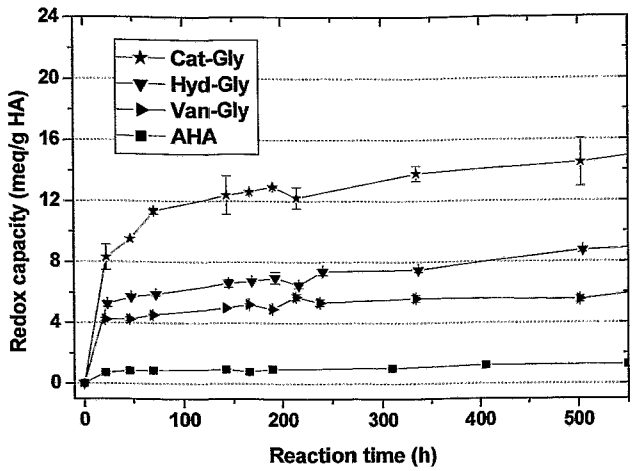

Fig. 3.6: Fe(III) redox capacities of synthetic HA based on the oxidation of different phenolic compounds in the presence of glycine.

Although synthetic HA type Van-Gly has a phenolic/acidic OH group content that is comparable to AHA (Tab. 3.5), all synthetic products exhibit higher redox capacities than AHA. The differences in the redox capacities of HA AHA and type Van-Gly points to structural differences of both HA influencing their redox behavior. Compared to the synthetic products of diphenols and glycine (Hyd-Gly, Cat-Gly), HA type Van-Gly has the lowest redox capacity which can be attributed to its lower phenolic/acidic OH group content. Among these, HA type Cat-Gly shows the highest Fe(III) redox capacity at pH 3 and also the highest phenolic/acidic OH group content. These results point to a correlation between the phenolic/acidic OH group content of the HA-like oxidation products from different phenolic precursor substances and glycine and their Fe(III) redox capacities.

Table 3.6 summarizes the Fe(III) redox capacities at pH 3 after about 3 weeks for all HA under investigation. From it it becomes obvious that synthetic HA type Cat-Gly shows the highest Fe(III) redox capacity under the considered experimental conditions. It is about twelve times higher than that of AHA.

Tab. 3.6: Fe(III) redox capacities for different synthetic HA in comparison to AHA at pH 3 after about 3 weeks reaction time.

HA	Redox capacity [a] (meq/g HA)
Hyd (batch R9/01)	9.6 ± 0.3
Hyd-Gly (batch R12/02)	8.8 ± 0.2
Hyd-Glu (batch R13/02)	10.7 ± 0.2
Cat-Gly (batch R18/02)	14.5 ± 1.6
Van-Gly (batch R5/02)	5.5 ± 0.2
M42 (batch M145)	6.1 ± 0.1
AHA (batch A2/98)	1.2 ± 0.1

[a] Mean values of duplicate measurements.

Referring the redox capacities of the HA to their phenolic/acidic OH group content, it becomes possible to draw conclusions concerning the kind of the redox active, i.e. electron-transferring, functional groups. In Fig. 3.7 the redox capacities of all studied HA after about 3 weeks are compared to their phenolic/acidic OH group contents. In contrast to HA AHA, all synthetic HA show redox capacities at pH 3 that are higher than their phenolic/acidic OH group contents. This result indicates that there are additional HA functional groups or other redox processes than the single oxidation of phenolic OH groups contributing to the reduction of Fe(III) within 3 weeks reaction time. For AHA the redox capacity is lower than its amount on phenolic/acidic OH groups which points to the fact that not all of these functional groups are contributing to the redox process.

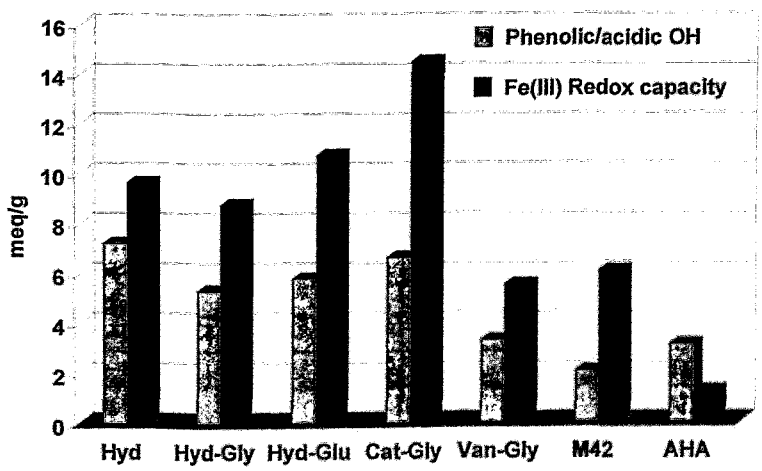

Fig. 3.7: Fe(III) redox capacities of the studied HA at pH 3 after 3 weeks reaction time in comparison to their phenolic/acidic OH group contents.

Based on the results of the Fe(III) redox capacity measurements at pH 3 HA type Hyd-Gly, Hyd-Glu and Cat-Gly were chosen as reference materials for HA model substances with pronounced redox functionalities. Therefore, they were additionally characterized with regard to their redox properties in the alkaline pH range.

Fe(III) redox capacities at pH 9.2

Figure 3.8 shows the ferricyanide redox capacities of HA type Hyd-Gly, Hyd-Glu and Cat-Gly as a function of time. They are compared to those of HA type M42 and AHA. The measured redox capacities at pH 9.2 after about 3 weeks are listed in Tab. 3.7.

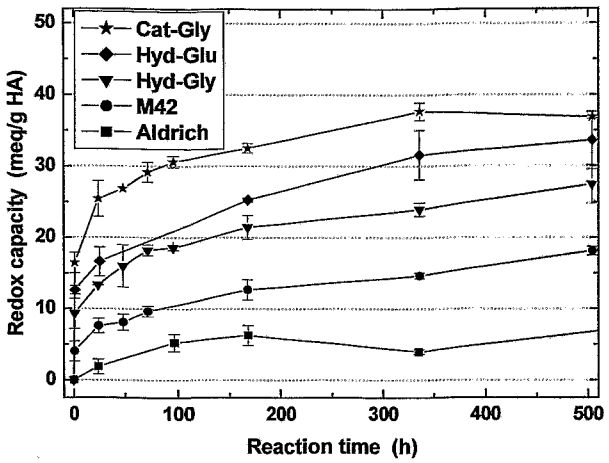

Fig. 3.8: Fe(III) redox capacities of synthetic HA based on the oxidation of hydroquinone and catechol at pH 9.2 in comparison to HA type M42 and AHA.

Tab. 3.7: Fe(III) redox capacities for different synthetic HA in comparison to AHA at pH 9.2 after about 3 weeks reaction time.

HA	Redox capacity [a] (meq/g HA)
Hyd-Gly (batch R12/02)	27.5 ± 2.7
Hyd-Glu (batch R13/02)	33.6 ± 4.0
Cat-Gly (batch R18/02)	36.9 ± 0.2
M42 (batch M145)	18.1 ± 0.6
AHA (batch A2/98)	7.2 ± 1.9

[a] Mean values of duplicate measurements.

From Fig. 3.8 and Tab. 3.7 it becomes obvious that all studied HA show higher Fe(III) redox capacities at pH 9.2 than at pH 3. Even at pH 9.2, all HA-like oxidation products from hydro-

quinone and catechol are characterized by higher redox capacities than AHA and M42 which can be ascribed to their higher phenolic/acidic OH group contents. The highest redox capacity at pH 9.2 exhibits HA type Cat-Gly. This result is comparable to that at pH 3. Figure 3.9 displays the Fe(III) redox capacities of the HA at pH 9.2 after about 3 weeks in comparison to their phenolic/acidic OH group contents.

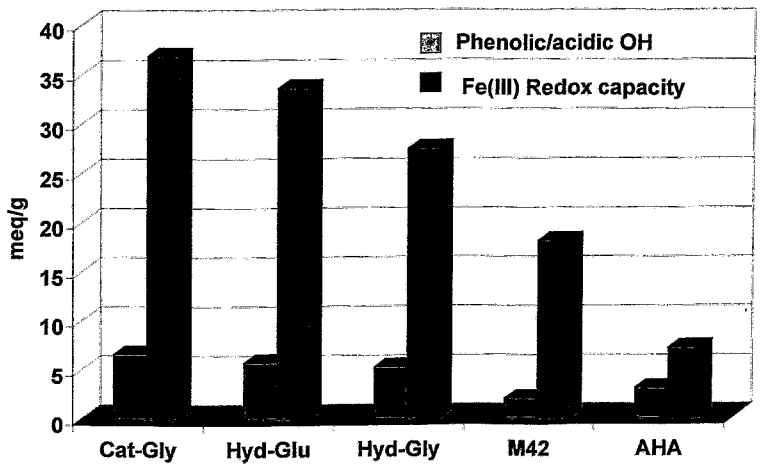

Fig. 3.9: Fe(III) redox capacities of the studied HA at pH 9.2 after 3 weeks reaction time in comparison to their phenolic/acidic OH group contents.

Also at pH 9.2, all HA show significantly higher redox capacities than those which would be expected assuming that only phenolic OH groups contribute to the reduction of Fe(III). From that it can be concluded again, that there are further processes than the single oxidation of phenolic OH groups or further HA functional groups that are also contributing to the reduction of Fe(III).

From all characterization results the conclusion can be drawn that it is possible to synthesize HA-like substances with pronounced redox functionalities by oxidation of phenolic compounds in the presence or absence of amino acids. By variation of the starting materials synthetic HA with varying elemental, functional and structural properties can be obtained.
Applying these HA model substances further studies on the redox properties of humic substances and on the redox stability of actinide humate complexes were performed. These are described in chapter 4 and 5, respectively.

4 Studies on the influence of phenolic OH groups on the redox behavior of natural and synthetic humic acids

The redox behavior of HA is ascribed to the system hydroquinone-quinone and the oxidation of phenolic OH groups (Fig. 3.3). However, the Fe(III) redox capacities at pH 3 and pH 9.2 that were measured for the HA-like oxidation products of phenolic compounds (see chapter 3.3.2) and also for HA type M42 and AHA (pH 9.2) are higher than those which would be expected assuming that only phenolic OH groups contribute to the reduction of Fe(III). In order to characterize the role of phenolic/acidic OH groups on the redox behavior of HA type Hyd-Gly, Hyd-Glu, Cat-Gly, M42 and AHA, we synthesized the corresponding HA with blocked phenolic/acidic OH groups by methylation with diazomethane (cf. 3.2). Applying these modified HA we determined the Fe(III) redox capacities at pH 3 (comparable to [29]) and at pH 9.2. We compared the results with those of the corresponding unmodified, original HA.

Tab. 4.1: Functional group contents of HA before and after modification with diazomethane.

HA	Modification	COOH (meq/g)	Phenolic/acidic OH (meq/g)	Phenolic/acidic OH : COOH
Hyd-Gly (batch R12/02)	Original	4.30 ± 0.14	5.3 ± 0.7	1.23
	Blocked phenolic/acidic OH	2.99 ± 0.10	1.5 ± 0.1	0.50
Hyd-Glu (batch R13/02)	Original	3.63 ± 0.20	5.8 ± 0.2	1.60
	Blocked phenolic/acidic OH	2.67 ± 0.03	1.4 ± 0.1	0.52
Cat-Gly (batch R18/02)	Original	4.16 ± 0.04	6.6 ± 0.7	1.59
	Blocked phenolic/acidic OH	2.88	1.3 ± 0.1	0.45
M42 (batch M145)	Original	3.76 ± 0.09	2.0 ± 0.2	0.53
	Blocked phenolic/acidic OH	3.12 ± 0.07	0.5	0.16
AHA (batch A2/98)	Original	4.49 ± 0.14	3.1 ± 0.1	0.69
	Blocked phenolic/acidic OH	2.67 ± 0.01	0.5	0.19

Table 4.1 summarizes the functional group contents of the studied unmodified and modified HA with blocked phenolic OH groups (HA-PB). Due to the modification with diazomethane all HA show significantly lower phenolic/acidic OH group contents. The amounts on these functional groups were decreased by 72 to 84 %. For all HA a lowering of the carboxyl group content due to the modification was observed. This could be due to an incomplete hydrolysis

of the carbonic methyl esters as already discussed in chapter 3.2. However, the molar ratio of phenolic/acidic OH to carboxyl groups is decreased for all HA. Therefore, we were able to apply these modified HA for the study of the influence of phenolic OH groups on the redox behavior of HA.

Figure 4.1 shows exemplary for the unmodified and modified HA type Hyd-Glu the Fe(III) redox capacities at pH 3 and pH 9.2. In Tab. 4.2 the results for all studied HA are listed.

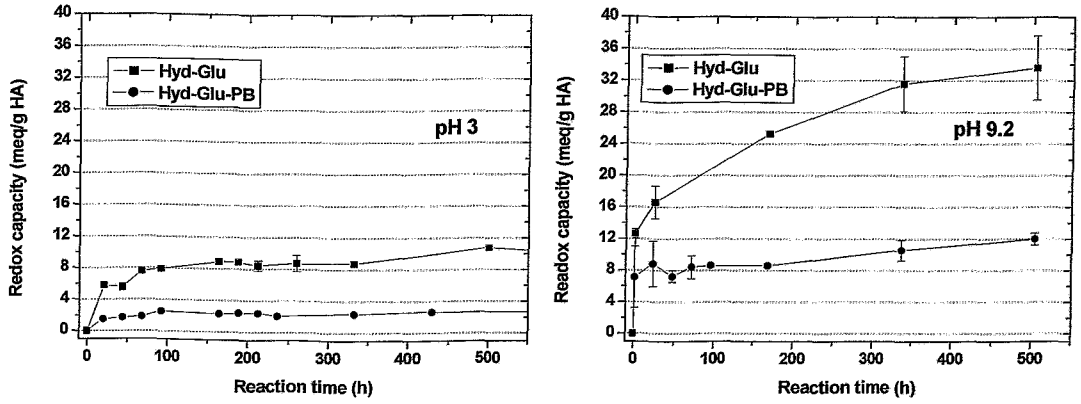

Fig. 4.1: Redox capacities of the unmodified and modified HA type Hyd-Glu with blocked phenolic/acidic OH groups.

Tab. 4.2: Redox capacities of the unmodified and modified HA after a reaction time of about 3 weeks.

HA	Modification	Fe(III) redox capacity at pH 3 [a] (meq/g HA)	Fe(III) redox capacity at pH 9.2 [a] (meq/g HA)
Hyd-Gly (batch R12/02)	Original	8.8 ± 0.2	27.5 ± 2.7
	Blocked phenolic/acidic OH	3.0 ± 0.2	10.1 ± 1.8
Hyd-Glu (batch R13/02)	Original	10.7 ± 0.2	33.6 ± 4.0
	Blocked phenolic/acidic OH	2.6 ± 0.1	12.0 ± 0.8
Cat-Gly (batch R18/02)	Original	14.5 ± 1.6	36.9 ± 0.2
	Blocked phenolic/acidic OH	2.7 ± 0.2	13.4 ± 0.1
M42 (batch M145)	Original	6.1 ± 0.1	18.1 ± 0.6
	Blocked phenolic/acidic OH	1.8 ± 0.1	7.6 ± 1.2
AHA (batch A2/98)	Original	1.2 ± 0.1	7.2 ± 1.9
	Blocked phenolic/acidic OH	0.5 ± 0.1	3.4 ± 1.4

[a] Mean values of duplicate measurements.

From Fig. 4.1 and Tab. 4.2 it becomes obvious that all modified HA with blocked phenolic/acidic OH groups show significant lower redox capacities at pH 3 and pH 9.2 than the corresponding unmodified, original HA. The observed decrease of the redox capacities at pH 3 is in agreement with first data described by Mack [29].

Due to the modification, the phenolic/acidic OH group content decreases, for instance, for HA type Hyd-Glu by 76 %. As a consequence of that the Fe(III) redox capacity at pH 3 and pH 9.2 is reduced by 76 % and 64 %, respectively. These results indicate that phenolic/acidic OH groups play a major role in the redox behavior of the studied HA-like oxidation product from hydroquinone. However, also for the modified HA Fe(III) redox capacities were determined that are higher than their remaining phenolic/acidic OH group contents, which is depicted in Fig. 4.2.

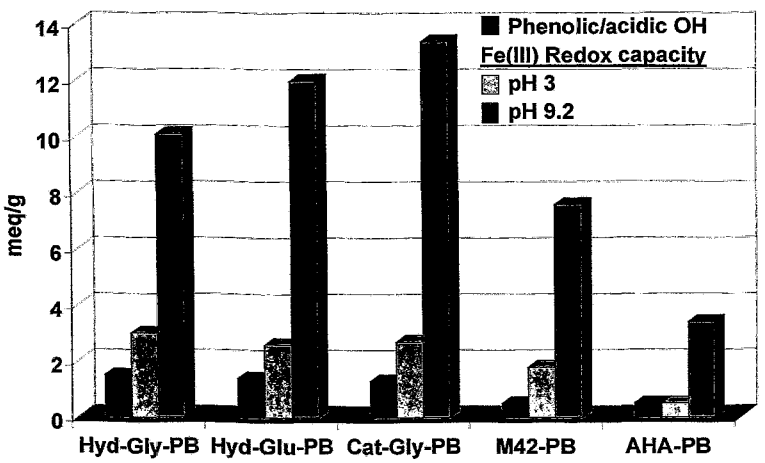

Fig. 4.2: Redox capacities of the modified HA in comparison to their phenolic/acidic OH group contents.

At pH 3, all modified synthetic HA show redox capacities that are slightly increased compared to those which would be expected assuming that only phenolic OH groups contribute to the redox process. In contrast to that, HA AHA-PB exhibits a redox capacity that is comparable to its amount on phenolic/acidic OH groups. However, at pH 9.2 all studied modified HA show significantly higher redox capacities than expected. These results support the assumption that there are other processes than the single oxidation of phenolic OH groups and/or other functional groups that are also contributing to the reduction of Fe(III), especially in the alkaline pH range.

The oxidation of phenols by $[Fe(CN)_6]^{3-}$ proceeds via intermediate phenoxy radicals that can undergo coupling reactions to various, often complex products. Tautomerization of the coupled products can result in a regeneration of phenolic hydroxyl groups, which may undergo further oxidation reactions. The oxidation rate is higher in alkaline solution [e.g., 32-34]. In addition to that, it is possible that aldehydes, ketones and nitroalkanes can be oxidized by $[Fe(CN)_6]^{3-}$ in alkaline solution [32]. Due to the complicated nature of HA, such secondary reactions could occur during the reduction of $[Fe(CN)_6]^{3-}$ by HA. Thus, this could result in the observed redox capacities that are higher than the phenolic/acidic OH group content of the investigated HA.

From these studies we conclude that phenolic/acidic OH groups play a significant role for the redox behavior of the studied synthetic (HA-like oxidation products of diphenolic compounds and a HA-like melanoidin) and natural HA. However, there exist other processes than the single phenol oxidation or other HA functional groups that are also contributing to the redox properties of the studied substances.

5 Studies on the redox stability of uranium(VI) complexes with synthetic and natural humic acids

In order to further improve the knowledge on the redox stability of actinide humate complexes as well in continuation of the characterization of the HA-like oxidation products from phenolic compounds described in chapter 3.3.2, we performed studies on the redox stability of U(VI) humate complexes. For this investigation we applied synthetic HA type Hyd-Glu and Cat-Gly (see chapter 3.3.2). Both model substances show significantly higher Fe(III) redox capacities than natural HA AHA. The studies were performed according to that published by Abraham [2], where the redox stability of U(VI) in the presence of lignin, wood degradation products and natural HA (e.g., unpurified natural HA from Aldrich) was investigated. For the first time, it was found in this investigation, that these organic materials are able to reduce U(VI) starting at pH values higher than pH 4.5. The direct spectroscopic proof for the occurrence of U(IV) in uranium solutions with lignin and wood degradation products at pH 9 and pH 8, respectively, was successful.

5.1 Experimental

The redox stability of U(VI) humate complexes of HA type Hyd-Glu, Cat-Gly and AHA was studied at pH 9 in 0.1 M $NaClO_4$ solutions. For that, U(VI) humate solutions with initial U(VI) and HA concentrations of $1 \cdot 10^{-4}$ M and 0.4 g/L, respectively, were prepared under nitrogen atmosphere applying CO_2-free solutions. The pH value of the samples was set to pH 9.0 using NaOH and $HClO_4$ solutions. In order to keep the pH value of the solutions constant during the experiment it was periodically checked and readjusted. The samples were stored under exclusion of light.

Laser-induced photoacoustic spectroscopy (LIPAS) was applied for the direct spectroscopic detection of U(IV) in the sample solutions. A tunable laser system was used. It is described in detail in [35]. The wavelength range between 600 and 675 nm was studied. For sample preparation 1 mL 6 M H_2SO_4 was added to 5 mL of the sample solutions. The addition of H_2SO_4 effects the precipitation of HA, the decomposition of possibly formed U(IV) humate complexes as well as the stabilization of U(IV) in the solutions in form of the U(IV) sulfate complex. After acidification, the HA precipitates were separated by centrifugation and the supernatants were studied by LIPAS.

5.2 Results and discussion

In Fig. 5.1 the photoacoustic spectra of the studied solutions after different reaction times are shown together with the peak deconvolution of the spectra. Comparing the spectra it becomes obvious that the spectra of the synthetic products are characterized by a high background absorption. This is due to an incomplete HA exclusion from the solutions which results in a HA contribution to the obtained absorption signal. However, from these spectra it becomes clear that HA AHA exhibits no absorption signals in the studied wavelength range, whereas for both synthetic products two absorption bands were detected. Thus, we conclude that after 92 days reaction time no detectable U(IV) concentration (detection limit: 10^{-5}-10^{-6} mol/L [2]) was formed by the possibly occurring U(VI) reduction by HA AHA. In absence of HA, the solvated U^{4+} ion shows characteristic absorption maxima at 629.5 nm, 649.1 nm and 671.7 nm [36]. These absorption wavelengths are close to that detected in the solutions with synthetic HA type Hyd-Glu and Cat-Gly after different reaction times. This result points to the occurrence of detectable quantities of U(IV) in the solutions with the HA-like oxidation prod-

ucts from hydroquinone and catechol. Therefore, it can be concluded that U(VI) was reduced by both HA model substances. The shift of the absorption bands could be due to the formation of U(IV) sulfate complexes in the studied solutions. Similar peak shifts were observed by Geipel et al. [36] for U(IV) complexes with arsenate. The spectra which were obtained for the synthetic products are similar to that of an uranium solution with wood degradation products published in [2], where the reduction of U(VI) by these substances was found.

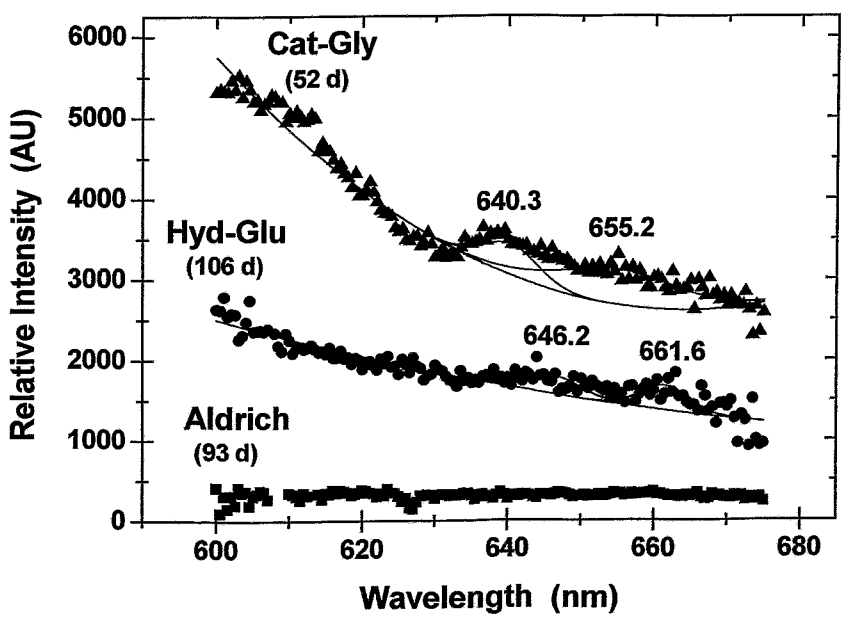

Fig. 5.1: Photoacoustic spectra of the studied HA solutions (starting conditions: $[UO_2^{2+}]$: $1 \cdot 10^{-4}$ mol/L, [HA]: 0.4 g/L, 0.1 M $NaClO_4$, pH 9.0). The numbers in brackets indicate the equilibration time of the samples.

From our spectroscopic results we conclude that the synthetic HA with pronounced redox functionalities show both higher Fe(III) and U(VI) redox capacities than HA AHA. The obtained results represent a first qualitative and direct spectroscopic proof for the reduction of uranium(VI) by HA. Further studies are performed in order to quantify the U(VI) redox capacities of the HA alike oxidation products from hydroquinone (Hyd-Glu) and catechol (Cat-Gly).

6 Investigations on the actinide complexation by humic substances

6.1 Structural studies on plutonium(III), thorium(IV), neptunium(IV) and neptunium(V) humate complexes by means of XAFS spectroscopy

Humic substances (humic acids and fulvic acids) are known for their strong complexing ability towards radionuclides thereby influencing their migration behavior. Therefore, to understand and predict the mobility of actinides in natural aquifer systems, amongst others, information on the coordination chemistry of the actinides in humate and fulvate complexes is necessary. We studied the coordination environment of Pu(III), Th(IV), Np(IV) and Np(V) in complexes with HA and fulvic acid (FA) by means of X-ray absorption fine structure (XAFS) spectroscopy. This includes the X-ray absorption near-edge structure (XANES) spectroscopy and the extended X-ray absorption fine structure (EXAFS) spectroscopy. The XANES spectroscopy provides information on the electronic structure and the molecular symmetry of the absorbing atom and the EXAFS spectroscopy contains information on coordination numbers and bond lengths to neighbor atoms [37].

Bio-Rex70 was used as reference substance to study the nature of metal complexation sites in humic substances further. Bio-Rex70 is a cation exchange resin that, in contrast to humic substances, has no phenolic OH groups but exclusively carboxyl groups as functional groups capable of binding metal ions. Thus, Th(IV), Np(IV) and Np(V) sorbates onto Bio-Rex70 were studied to determine structural parameters for the interaction of the respective actinide ion with carboxyl groups.

In case of Np(V), the influence of HA phenolic/acidic OH groups on the interaction between Np(V) and HA was studied at pH 7 applying modified HA with blocked phenolic/acidic OH groups in addition to the respective unmodified HA.

The structural parameters determined for the actinide humate complexes are further compared with structural parameters of the respective aqueous actinide ions and of solid actinide carboxylate complexes given in the literature.

6.1.1 Experimental

Sorbents

Both natural and synthetic humic substances were applied for the study. The natural humic substances were Kranichsee FA (KFA) that was isolated from surface water of the mountain

bog 'Kleiner Kranichsee' (Johanngeorgenstadt, Saxony, Germany) [38] as well as the commercially available, purified Aldrich HA (AHA). The synthetic HA model substances were the HA type M1 [10,39] and type M42 (see chapter 3.1). Furthermore, from AHA, M1 and M42 also modified HA with blocked phenolic/acidic OH groups (AHA-PB, M1-PB, M42-PB) (see chapter 3.2 and [15]) were applied. Bio-Rex70 (Bio-Rad, München, Germany) was used as reference substance.

Th(IV) samples

^{232}Th(IV) samples were prepared from AHA and from Bio-Rex70 at pH 1 (0.1 M $HClO_4$). The Th loading of the resulting wet pastes was 40.8 mg Th/g AHA and 1.9 mg Th/g Bio-Rex70 which corresponds to a Th loading of 14.7 % and 0.3 % of the proton exchange capacity (PEC) of the sorbents.

Np(IV) samples

A ^{237}Np(IV) stock solution was prepared by electrochemical reduction of a Np(V) solution to Np(III) followed by air oxidation to Np(IV). The tetravalent oxidation state of Np was verified by near infrared (NIR) absorption spectroscopy. Np(IV) samples were prepared from AHA, KFA, M42 and from Bio-Rex70 at pH 1 (0.1 M $HClO_4$) under inert gas conditions. The Np loading of the resulting wet pastes was between 4 and 41 mg Np/g sorbent (0.7 % to 15 % of the PEC of the sorbents).

Np(V) samples

^{237}Np(V) complexes were prepared from the unmodified HA AHA, M1 and M42 and from modified HA AHA-PB, M1-PB and M42-PB with blocked phenolic/acidic OH groups as well as from Bio-Rex70. The Np(V) humate solutions were prepared at pH 7 under inert gas conditions with Np and HA concentrations of 0.88-1.04 mmol/L and of 8.1-27.5 g/L, respectively (ionic strength: 0.1 M $NaClO_4$). The Np loading was between 2.3 and 2.8 % of the PEC of the sorbents. The Np(V)-Bio-Rex70 sorbate was prepared at pH 7 in 0.1 M $NaClO_4$. The Np loading of the resulting wet paste was 121.3 mg Np/g Bio-Rex70 (5.1 % PEC).

Pu(III) samples

^{242}Pu was purified in the tetravalent oxidation state by anion exchange chromatography using TEVA resin™. Purified Pu(IV) was electrochemically reduced to Pu(III). The trivalent oxidation state of Pu was verified by NIR absorption spectroscopy. Pu(III) samples were prepared from KFA and from M42 at pH 1 (0.1 M $HClO_4$) under inert gas conditions. The Pu loading of the resulting wet pastes of KFA and M42 was 11.6 and 3.9 mg Pu per g sorbent, respectively.

The experimental conditions are described in more detail in Schmeide et al. [40,41] and Sachs et al. [42].

XAFS measurements and data analysis

The XAFS measurements were carried out at the Rossendorf Beamline (ROBL) [43] at the European Synchrotron Radiation Facility (ESRF) in Grenoble, France. The actinide L_{III}-edge X-ray absorption spectra were collected in fluorescence mode (Th(IV) samples, Pu(III) samples, Np(V) humates) and transmission mode (Np(IV) samples, Np(V)-Bio-Rex70), respectively, at room temperature. A Si(111) double-crystal monochromator was used in fixed-exit mode. Several EXAFS scans were collected from each sample and averaged.

Data analysis was performed according to standard procedures [37] using the EXAFSPAK software [44]. The program FEFF6 [45] was used to calculate theoretical scattering amplitudes and phase-shift functions.

The EXAFS oscillations were fitted to the EXAFS equation using one coordination shell with oxygen as backscatterer in case of Th(IV), Np(IV) and Pu(III). In case of Np(V), a two-shell fit with axial and equatorial oxygen atoms (O_{ax}, O_{eq}) as backscatterers was used. The multiple scattering along the neptunyl unit (O_{ax}-Np-O_{ax}) was also included in the fit.

6.1.2 Results and discussion

Th(IV) humate and Bio-Rex70 complexes

The raw Th L_{III}-edge k^3-weighted EXAFS spectra and the corresponding Fourier transforms (FT) of the Th(IV) complexes with AHA and Bio-Rex70 are shown in Fig. 6.1. Both the

EXAFS spectra and the FT of the samples are comparable. The FT are dominated by a peak at about 1.8 Å representing oxygen atoms coordinated to Th(IV).

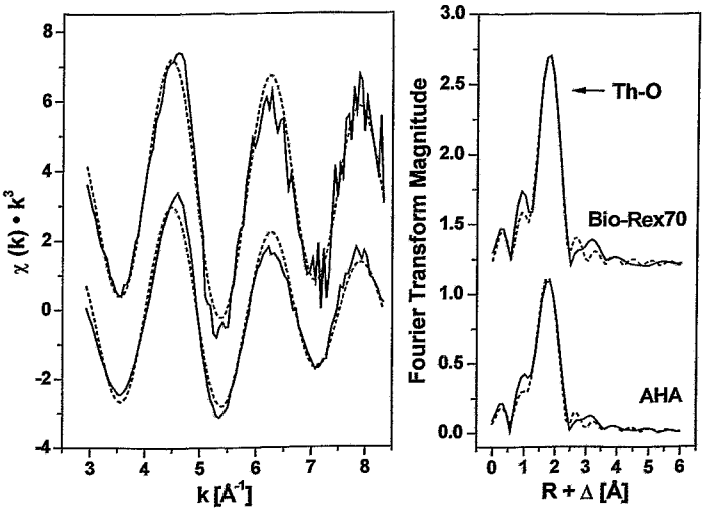

Fig. 6.1: Th L_{III}-edge k^3-weighted EXAFS spectra and corresponding FT of Th(IV) samples. Solid lines: experiment, dashed lines: fit.

In Tab. 6.1 the structural parameters determined for the Th(IV) complexes are summarized such as coordination number (N), bond length (R) and Debye-Waller factor (σ^2) obtained from fits to the EXAFS equation. The coordination numbers and Th-O bond lengths of Th(IV)-AHA and Th(IV)-Bio-Rex70 are comparable. In both samples, Th(IV) is surrounded by 11 oxygen atoms at a distance of 2.44 Å. Since Bio-Rex70 has no phenolic OH groups but exclusively carboxyl groups as functional groups capable of binding metal ions, it can be concluded that the interaction between AHA and Th(IV) is dominated by HA carboxyl groups under the experimental conditions applied. This result was expected since at pH 1 the phenolic OH groups of the humic substances are fully protonated. The larger EXAFS Debye-Waller factor determined for the oxygen coordination shell of Th(IV)-AHA in comparison to those of Th(IV)-Bio-Rex70 and the aqueous Th(IV) ion points to a broader distribution of Th-O bond lengths in the Th(IV) humate complex.

Tab. 6.1: EXAFS structural parameters of Th(IV) complexes in comparison to literature data of Th(IV) samples.

Sample	Th-O			ΔE_0 (eV)	Ref.
	N	R (Å)	σ^2 (Å^2)		
Th(IV)-AHA	10.6 ± 1.5	2.44 ± 0.01	0.013	-17.3	
Th(IV)-Bio-Rex70	11.0 ± 2.1	2.45 ± 0.02	0.009	-17.3	
Th(IV)-AHA	10.1	2.43	0.013	1.0	[46]
Th(IV)-Bio-Rex70	9.4	2.44	0.012	1.0	[46]
$Th(H_2O)_x^{4+}$	10.8 ± 0.5	2.45 ± 0.01	0.007	4.0	[47]

The 95 % confidence limits are given for N and R as estimated by EXAFSPAK.

Within the experimental error, the structural parameters determined for the Th(IV) humate and Bio-Rex70 complexes agree with those determined by Denecke et al. [46]. Furthermore, the data of Th(IV)-AHA are comparable to those of the aqueous Th(IV) ion [47]. This shows that the interaction between Th(IV) and HA carboxyl groups induces no shortening of the Th-O bond length. Furthermore, since no carbon atoms of the binding HA carboxylate groups can be detected, it is not possible to determine separate coordination numbers for carboxylate groups and water molecules coordinated to Th(IV) by EXAFS analysis.

To identify the binding mode (monodentate, bidentate or bridging) of HA carboxylate groups to Th(IV), the Th-O bond length of Th(IV) humate is compared with those of Th(IV) model compounds which contain carboxyl groups. The average Th-O bond length observed for monodentate coordinated carboxylate groups in various Th(IV) malonates [48] as well as in Th(IV) oxalate [49] is 2.42 ± 0.04 Å. This bond length is comparable to the bond length obtained for Th(IV)-AHA (2.44 ± 0.01 Å). This points to a predominant monodentate coordination of HA carboxylate groups to Th(IV).

Np(IV) humate and Bio-Rex70 complexes

The tetravalent oxidation state of Np and its stability in the humate and Bio-Rex70 complexes within the time of our experiment was verified by means of NIR absorption spectroscopy [40] and XANES spectroscopy. In Fig. 6.2, the XANES spectrum of Np(IV)-AHA is shown in comparison to that of the corresponding Np(V) sample. The spectrum of Np(IV) humate shows the characteristic near-edge features of Np(IV) compounds: A more intense 'white line' peak, but no additional shoulder on the high energy side of the 'white line' as generally observed for Np(V) samples. Identical spectral features were obtained for the Np(IV) complexes of KFA, M42 and Bio-Rex70.

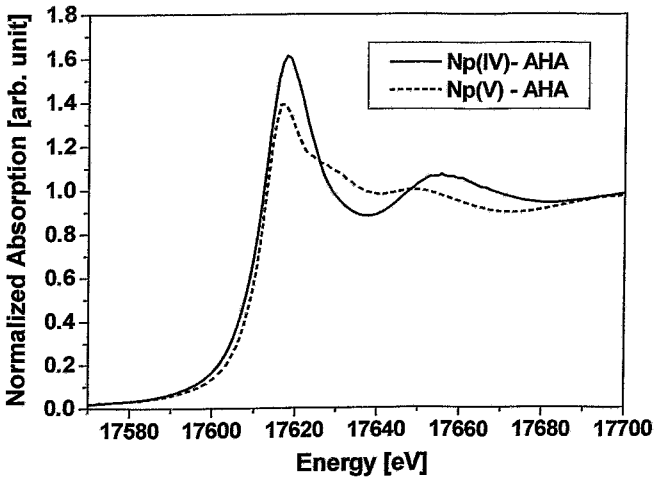

Fig. 6.2: Normalized Np L_{III}-edge XANES spectra.

The raw Np L_{III}-edge k^3-weighted EXAFS spectra and the corresponding FT of the Np(IV) samples are shown in Fig. 6.3. Both the EXAFS oscillations and the FT of all Np(IV) complexes are similar. The FT are dominated by one peak at about 1.7 Å representing one coordination shell with oxygen as backscatterer. No Np-Np contributions were observed in the spectra, i.e., polynuclear Np species did not form.

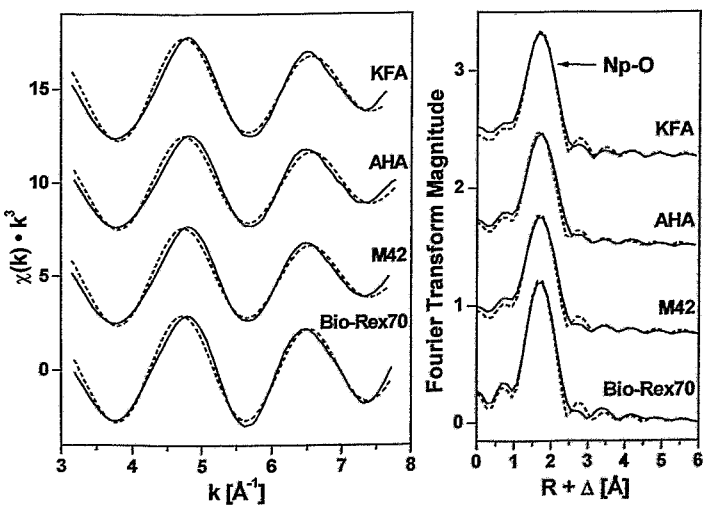

Fig. 6.3: Np L_{III}-edge k^3-weighted EXAFS spectra and corresponding FT of Np(IV) samples. Solid lines: experiment, dashed lines: fit.

The EXAFS structural parameters determined for the Np(IV) complexes are compiled in Tab. 6.2 and compared to literature data of Np(IV) samples.

In the Np(IV) humate complexes, the Np(IV) ion is surrounded by about 11 oxygen atoms at a distance of 2.36 Å. Comparable parameters are determined for the Np(IV) complex with Bio-Rex70. This again verifies the dominance of carboxyl groups for the complexation of actinide ions by humic substances at pH 1 (cf. Th(IV) humates).

Tab. 6.2: EXAFS structural parameters of Np(IV) complexes in comparison to literature data of Np(IV) samples.

Sample	Shell	N	R (Å)	σ^2 (Å^2)	ΔE_0 (eV)	Ref.
Np(IV)-KFA	Np-O	11.3 ± 1.7	2.36 ± 0.01	0.0162	-11.1	
Np(IV)-AHA	Np-O	10.1 ± 1.7	2.36 ± 0.01	0.0159	-11.1	
Np(IV)-M42	Np-O	11.0 ± 1.7	2.36 ± 0.01	0.0166	-11.1	
Np(IV)-Bio-Rex70	Np-O	10.2 ± 1.3	2.37 ± 0.01	0.0127	-11.1	
$Np(H_2O)_x^{4+}$ in 1 M $HClO_4$	Np-O	9 ± 1	2.37 ± 0.02	0.007		[50]
$Np(H_2O)_x^{4+}$ in 1 M HCl	Np-O	11.2 ± 1.1	2.40 ± 0.012	0.0075		[51]
$Np(H_2O)_x^{4+}$ in 2 M H_2SO_4	Np-O Np-S	11 ± 1 2.2 ± 0.9	2.39 ± 0.01 3.07 ± 0.02	0.0118 0.0070		[43]

The 95 % confidence limits are given for N and R as estimated by EXAFSPAK.

Compared to the aqueous Np(IV) ion in hydrochloric or sulfuric medium [43,51], the coordination number of the humates is similar, only the Np-O bond length is shortened by about 0.04 Å due to humate complexation. A similar shortening of the bond length has been previously observed for U(VI) humate complexes ($R_{U\text{-}Oeq}$ = 2.37-2.39 Å) [23,52,53] compared to $UO_2(H_2O)_5^{2+}$ ($R_{U\text{-}Oeq}$ = 2.41 Å) [51] and can be interpreted as further evidence of actinide humate complex formation. However, as found for Th(IV), a differentiation between HA carboxylate groups and water molecules coordinated to the Np(IV) ion is not possible by means of EXAFS spectroscopy.

The comparison of the bond length determined for the Np(IV) humates with those of Np(IV) model compounds containing carboxyl groups shows that the bond length of the Np(IV) humates is smaller than found for bridging and chelate forming carboxylate groups in Np(IV) oxalate (R = 2.39 Å and 2.51 Å with an average of 2.45 Å) [54] or for bidentate binding carboxylate groups in Np(IV) formate (R = 2.50 Å) [55]. From this we conclude that the HA carboxylate groups are predominantly monodentate bound to Np(IV) ions.

The comparison of the structural parameters of Np(IV) humate and Bio-Rex70 complexes with those of the corresponding Th(IV) complexes shows that both tetravalent actinides are surrounded by 11 oxygen atoms. However, the Np-O bond length (2.36 ± 0.02 Å) is about 0.08 Å shorter than the Th-O bond length (2.44 ± 0.02 Å). This difference approximates the

difference of the effective ionic radii of Np^{4+} (1.02 ± 0.02 Å [56]) and Th^{4+} (1.08 ± 0.02 Å, [56]) in aqueous solution which is 0.06 ± 0.02 Å.

Np(V) humate and Bio-Rex70 complexes

For all Np(V) humates the complexation of NpO_2^+ by HA was verified by means of NIR absorption spectroscopy [42].

The raw Np L_{III}-edge k^2-weighted EXAFS spectra and the corresponding FT of the Np(V) complexes are shown in Fig. 6.4. The FT show two Np-O coordination shells (Np-O_{ax}, Np-O_{eq}). No Np-Np interactions are indicated in the FT. The structural parameters determined for the Np(V) complexes are summarized in Tab. 6.3 and compared to literature data of the aqueous Np(V) ion.

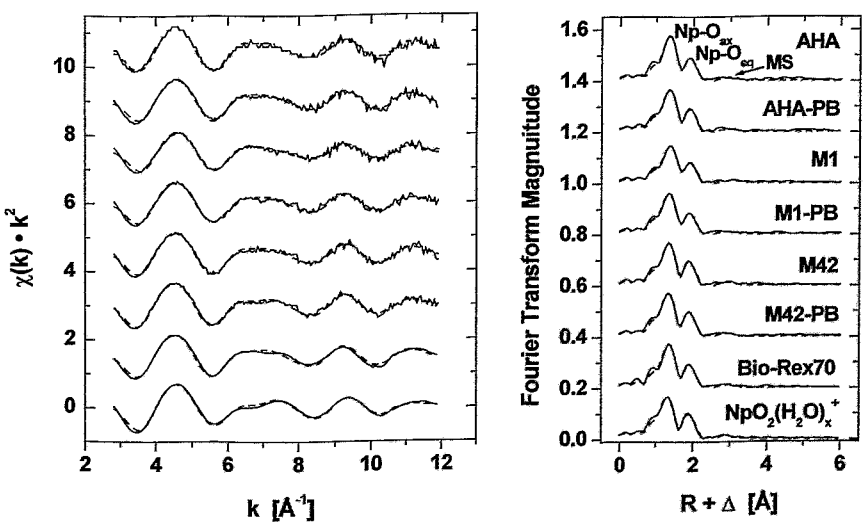

Fig. 6.4: Np L_{III}-edge k^2-weighted EXAFS spectra and corresponding FT of Np(V) samples. Solid lines: experiment, dashed lines: fit, MS: multiple scattering along the neptunyl unit.

Within the experimental error, identical structural parameters were determined for Np(V) humates prepared from original HA and from modified HA with blocked phenolic/acidic OH groups. From this it can be concluded that the blocking of the phenolic/acidic OH groups of the HA has no influence on the local structure around the Np(V) ion in the Np(V) humates. Furthermore, the structural data of the Np(V) humates are also comparable to those of Np(V)-Bio-Rex70. This indicates that carboxylate groups dominate the interaction between Np(V)

and HA at pH 7. However, a contribution of HA phenolic/acidic OH groups to the complexation of Np(V) ions cannot completely be excluded by EXAFS analysis, since the EXAFS results represent average values over all interactions between Np(V) and HA functional groups. There is the possibility that phenolic OH groups interacting with Np(V) show equatorial bond lengths that are similar to those of carboxylate groups.

Tab. 6.3: EXAFS structural parameters of Np(V) complexes in comparison to literature data of the aqueous Np(V) ion.

Sample	Np-O_{ax}			Np-O_{eq}			ΔE_0
	N	R (Å)	σ^2 (Å^2)	N	R (Å)	σ^2 (Å^2)	(eV)
Np(V)-AHA	2.0 ± 0.3	1.85 ± 0.01	0.0017	2.8 ± 0.7	2.49 ± 0.02	0.0050	-8.1
Np(V)-AHA-PB	2.0 ± 0.3	1.85 ± 0.01	0.0021	2.3 ± 0.6	2.49 ± 0.01	0.0028	-7.7
Np(V)-M1	1.8 ± 0.3	1.86 ± 0.01	0.0026	2.6 ± 0.6	2.49 ± 0.02	0.0053	-6.4
Np(V)-M1-PB	2.0 ± 0.2	1.85 ± 0.01	0.0026	2.5 ± 0.6	2.49 ± 0.02	0.0043	-8.4
Np(V)-M42	1.9 ± 0.2	1.84 ± 0.01	0.0014	2.8 ± 0.6	2.48 ± 0.01	0.0041	-9.3
Np(V)-M42-PB	2.0 ± 0.2	1.84 ± 0.01	0.0020	2.8 ± 0.5	2.49 ± 0.01	0.0037	-10.0
Np(V)-Bio-Rex70	2.0 ± 0.2	1.85 ± 0.01	0.0017	2.7 ± 0.5	2.50 ± 0.01	0.0043	-8.8
$NpO_2(H_2O)_x^+$ [43]	2.0 ± 0.2	1.82 ± 0.01	0.0026	2.9 ± 0.4	2.49 ± 0.01	0.0038	-9.2
$NpO_2(H_2O)_x^+$ [51]	2	1.85	0.0018	5.0	2.50	0.007	

The 95 % confidence limits are given for N and R as estimated by EXAFSPAK.

The coordination number determined for the equatorial shell of Np(V) humate and Np(V)-Bio-Rex70 complexes as well as for the equatorial shell of the aqueous ion of Np(V) [43] is smaller than the theoretically expected value of 5. Up to now, this cannot be explained.

The equatorial Np-O bond lengths of the humates are comparable to the mean equatorial Np-O bond lengths of monodentate and/or bridging coordinated carboxylate groups in crystalline Np(V) carboxylate complexes reported in the literature (2.46 ± 0.04 Å) that are summarized in [42]. Moreover, the equatorial Np-O bond lengths of the humates are also comparable to the equatorial Np-O bond length of the aqueous Np(V) ion. Thus, a differentiation between monodentate/bridging carboxylate groups and water molecules is not possible. However, a predominant bidentate coordination of HA carboxylate groups to Np(V) can be excluded, since bidentate coordinated carboxylate groups in different crystalline Np(V) carboxylates show a mean equatorial Np-O bond length of 2.59 ± 0.08 Å (summarized in [42]) which is significantly longer.

Pu(III) humate complexes

The trivalent oxidation state of Pu and its stability in the complexes with humic substances within the time of the experiment was verified by means of XANES spectroscopy. In Fig. 6.5, the XANES spectra of Pu(III)-KFA and Pu(III)-M42 are shown in comparison to that of the aqueous ion of Pu(III) [59]. The energy scale of the spectra was calibrated with a Zr metal foil (Zr K edge at 17998 eV). The edge energy, determined as the inflection point of the edge, of the three spectra is identical (aqueous Pu(III) ion: 18059.0 eV, Pu(III) humates: 18059.2 eV). This confirms that the humate complexes contain exclusively Pu(III).

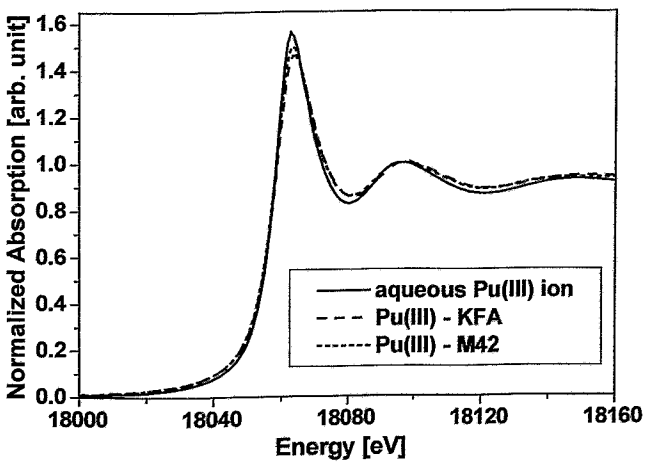

Fig. 6.5: Normalized Pu L_{III}-edge XANES spectra.

The raw Pu L_{III}-edge k^3-weighted EXAFS spectra and the corresponding FT of the Pu(III) humates are shown in Fig. 6.6. The FT indicate a single coordination shell (Pu-O) arising from the ligands.

The structural parameters determined for the Pu(III) complexes are summarized in Tab. 6.4 and compared to literature data of aqueous ions of Pu(III) and Pu(IV). In the Pu(III) humate complexes the Pu(III) ion is surrounded by about 7 oxygen atoms at a distance of 2.45 Å. The Pu-O bond length in the Pu(III) humate complexes is significantly longer than that of the aqueous Pu(IV) ion. Furthermore, no evidence for the formation of polynuclear Pu(IV) species was found in the EXAFS spectra. That means, the EXAFS structural parameters confirm the conclusion drawn from the XANES spectra namely that the humate complexes contain exclusively Pu(III).

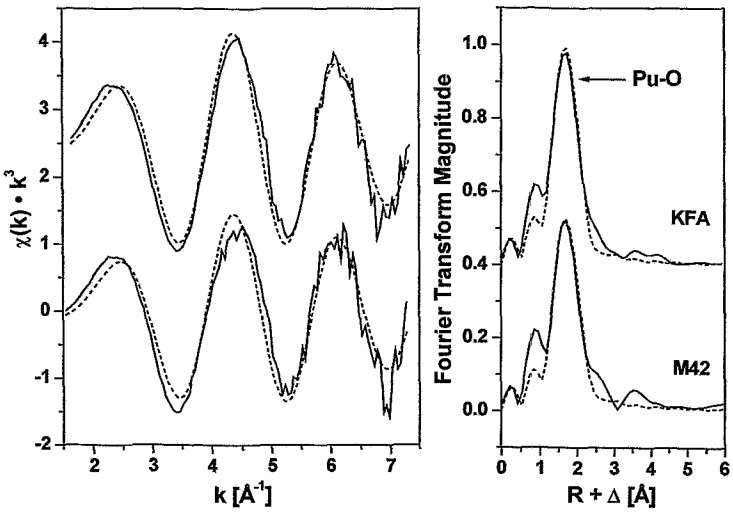

Fig. 6.6: Pu L_{III}-edge k^3-weighted EXAFS spectra and corresponding FT of Pu(III) samples. Solid lines: experiment, dashed lines: fit.

Tab. 6.4: EXAFS structural parameters of Pu(III) complexes in comparison to literature data of aqueous ions of Pu(III) and Pu(IV).

Sample	Shell	N	R (Å)	σ^2 (Å^2)	ΔE_0 (eV)	Ref.
Pu(III)-KFA	Pu-O	7.3 ± 1.2	2.45 ± 0.02	0.0150	-17.3	
Pu(III)-M42	Pu-O	6.1 ± 1.4	2.45 ± 0.02	0.0137	-17.0	
$Pu(H_2O)_x^{3+}$	Pu-O	7.6 ± 0.6	2.48 ± 0.01	0.0102	-16.8	[59]
$Pu(H_2O)_x^{4+}$	Pu-O	8	2.39	0.0118		[60]

The 95 % confidence limits are given for N and R as estimated by EXAFSPAK.

Within the experimental error, the coordination numbers determined for the Pu-O shell of the humate complexes agree well with the value reported for the aqueous Pu(III) ion in 1 M $HClO_4$ [59]. The bond length determined for the Pu(III) humate complexes is 0.03 Å shorter than that determined for the aqueous Pu(III) ion. This shortening of the bond length is similar to that observed for U(VI) and Np(IV) humates upon complexation of these actinides with the functional groups of the humic substances.

6.2 Studies on the influence of phenolic OH groups on the neptunium(V) complexation by humic acids

In order to further improve the knowledge on the influence of phenolic OH groups on the metal ion complexation by HA in neutral and alkaline solutions we continued our studies on the Np(V)-HA-complexation using modified HA with blocked phenolic OH groups. In continuation of our EXAFS investigations (chapter 6.1), which resulted in structural information on the near-neighbor surrounding of Np(V) in humate complexes, we determined and compared loading capacities and complexation constants of Np(V) complexes with unmodified and chemically modified (phenolic OH groups blocked) HA type M42 and Aldrich. These studies were performed by near-infrared (NIR) spectroscopy.

6.2.1 Experimental

Np(V) humate solutions were prepared under nitrogen atmosphere from natural HA Aldrich (AHA, batch A2/98), synthetic HA type M42 (batch M145), as well as modified HA AHA and M42 with blocked phenolic OH groups (AHA-PB, M42-PB). For synthesis and characterization of these HA see chapter 3.2.

In our experiments the HA concentration ([HA(I)] [11]) was held constant at $1 \cdot 10^{-3}$ mol/L and the Np(V) concentration was varied between $5.3 \cdot 10^{-5}$ and $1.3 \cdot 10^{-3}$ mol/L. The studies were performed at room temperature in 0.1 M $NaClO_4$ solutions at pH 7 for all HA and at pH 8 for AHA and AHA-PB. The samples were prepared from stock solutions of HA and NpO_2^+ (^{237}Np, $4.6 \cdot 10^{-3}$ M, 0.01 M HNO_3). The ionic strength was adjusted applying 1 M $NaClO_4$ solution. The total neptunium concentration in solution was determined by liquid scintillation counting (LSC, Beckman Instruments). NIR absorption spectra of all Np(V) humate solutions were recorded in the wavelength range between 950 and 1010 nm with the UV-Vis-NIR spectrophotometer CARY-5G (Varian).

The Np(V) species distribution in the absence of HA at pH 7 and pH 8 ([NpO_2^+]: $1 \cdot 10^{-5}$ M and $1 \cdot 10^{-3}$ M, 0.1 M $NaClO_4$, 0 % CO_2) was calculated with the program EQ3/6 [12] based on complex formation constants compiled in [61]. Under the considered conditions the NpO_2^+ ion dominates the Np(V) speciation. It occurs with a relative concentration of 100.00 % and 99.96 % at pH 7 and pH 8, respectively. Therefore, it can be concluded that NpO_2^+ is the Np(V) species which reacts with HA under the studied experimental conditions.

6.2.2 Results and discussion

The measured NIR absorption spectra represent the sum of the absorption signals of the uncomplexed NpO_2^+ ion (980 nm) and the Np(V) humate complex ($NpO_2HA(I)$, 985-989 nm depending on HA). The spectra were deconvoluted into single peaks for both species in order to determine their concentration in solution. Figure 6.7 shows a measured NIR absorption spectrum of a Np(V) solution with HA AHA and its deconvolution.

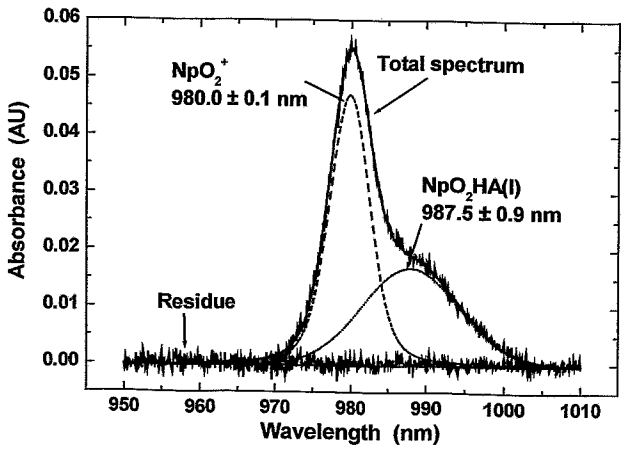

Fig. 6.7: NIR absorption spectrum of Np(V) in HA solution and its deconvoluted absorption bands (AHA, [HA(I)]: $1 \cdot 10^{-3}$ mol/L, $[NpO_2^+]$: $1.7 \cdot 10^{-4}$ mol/L, pH 7, 0.1 M $NaClO_4$).

The experimental data were evaluated with the metal ion charge neutralization model [11]. According to this model, NpO_2^+ occupies one proton exchanging site of the HA molecule [Eq. (6.1)]:

$$NpO_2^+ + HA(I) \rightleftharpoons NpO_2HA(I) \qquad (6.1)$$

where HA(I) represents the HA ligand and $NpO_2HA(I)$ stands for the neptunyl humate complex. The stability constant β is given by

$$\beta = \frac{[NpO_2HA(I)]}{[NpO_2^+]_{free} \cdot [HA(I)]_{free}} \qquad (6.2)$$

where $[NpO_2HA(I)]$ is the neptunyl humate complex concentration, $[NpO_2^+]_{free}$ the free NpO_2^+ concentration and $[HA(I)]_{free}$ the free HA ligand concentration [11]. This model introduces the loading capacity (LC, [Eq. (6.3)]) which represents the mole fraction of maximal available complexing sites of HA under the applied experimental conditions.

$$LC = \frac{[NpO_2HA(I)]_{max}}{[HA(I)]_{tot}} \tag{6.3}$$

$[NpO_2HA(I)]_{max}$ is the maximum concentration of NpO_2^+ that can be complexed by functional sites of HA and $[HA(I)]_{tot}$ stands for the total molar HA concentration [11]. Taking the LC into account the free HA concentration in solution can be determined according to [11] and the stability constant (β) can be described by Eq. (6.4).

$$\beta = \frac{[NpO_2HA(I)]}{[NpO_2^+]_{free} \cdot ([HA(I)]_{tot} \cdot LC - [NpO_2HA(I)])} \tag{6.4}$$

The LC is graphically determined by linear regression after rearranging Eq. (6.4) for the free NpO_2^+ ion concentration [11]. Considering the graphically determined LC, we computed a complexation constant for each experimental point.

Applying this model, the complexation behavior of HA can be described independently of the experimental conditions and the HA origin. From this it follows, that comparable complexation constants are determined for the complexation of a metal ion, e.g., Np(V), with different HA. Differences in the complexation behavior of various HA under the same experimental conditions are reflected in different LC values. A significant lower LC for HA with blocked phenolic/acidic OH groups should result, if the blocking of these HA functional groups has an influence on the complexation behavior of HA with Np(V) in the neutral and alkaline pH range.

Table 6.5 summarizes the spectroscopically determined complexation data (LC, log β) for the investigated HA at pH 7 and pH 8. Figure 6.8 shows, exemplary for modified and unmodified HA type M42, the mole ratios $[NpO_2HA(I)]/[HA(I)]_{tot}$ versus $[NpO_2^+]_{tot}/[HA(I)]_{tot}$ which illustrate the LC values.

Tab. 6.5: Complexation data for the complexation of Np(V) with unmodified and modified HA type M42 and AHA in comparison to literature data.

HA	pH	LC (%) [a]	log β [a]
AHA (batch A2/98)	7.0	10.0 ± 1.5	3.87 ± 0.19
	8.0	35.3 ± 3.7	3.59 ± 0.17
AHA-PB (batch M173)	7.0	6.5 ± 2.4	3.39 ± 0.15
	8.0	12.3 ± 2.6	3.46 ± 0.22
M42 (batch M145)	7.0	11.2 ± 1.1	3.50 ± 0.15
M42-PB (batch M171)	7.0	5.3 ± 1.0	3.48 ± 0.11
GoHy-573 [62]	7	9.9 ± 0.2	3.65 ± 0.03
	8	14.9 ± 0.3	3.68 ± 0.08
GoHy-573 [63]	7	13.0 ± 1.0	3.53 ± 0.05
	8	22.0 ± 1.5	3.61 ± 0.07
Aldrich [64]	8	32.4	3.7

[a] ± 3 σ.

Within the experimental errors, the studied HA show similar Np(V) complexation constants that are close to literature data for HA GoHy-573 [62,63] and Aldrich [64]. However, there are differences in the LC of HA AHA, M42 and GoHy-573 especially at pH 8. These could be explained by the different origin of the HA resulting in various complexation properties. The obtained LC for AHA at pH 8 agrees with that data reported by Seibert et al. [64].

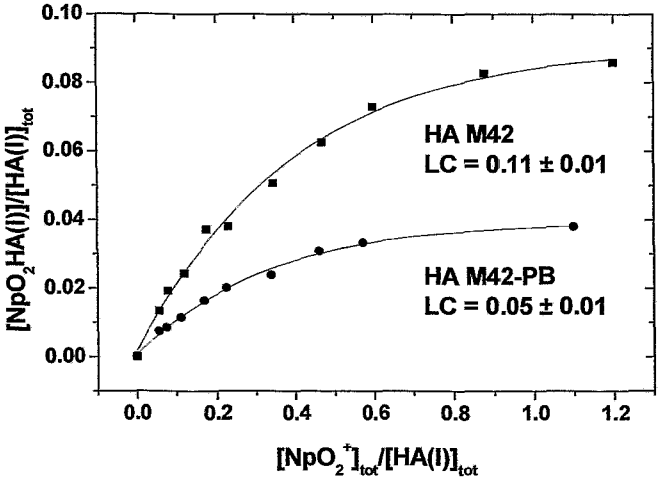

Fig. 6.8: Illustration of the Np(V) loading capacity (LC) of modified (M42-PB) and unmodified (M42) synthetic HA type M42 at pH 7.

Comparing the LC values of the corresponding modified and unmodified HA at pH 7 and pH 8 it becomes obvious that modified HA AHA-PB and M42-PB have significantly lower LC than the original, unmodified HA AHA and M42, respectively. Due to the modification of phenolic/acidic OH groups (75 % M42 and 84 % AHA, see Tab. 3.2) the LC of HA M42 and AHA at pH 7 decreases for 53 % and 35 %, respectively. The LC of AHA at pH 8 is reduced for 65 %. These results point to a decrease of the mole fraction of HA binding sites for the Np(V) complexation due to the blocking of phenolic/acidic OH groups. Thus, it can be concluded that phenolic/acidic OH groups are involved into the interaction between HA and Np(V) in the neutral and alkaline pH range. Comparable results were already found for the uranium(VI) complexation at pH 4 with various HA at pH 4 [15]. Although the blocking of phenolic/acidic OH groups decreases the number of HA complexing sites, the structural parameters of Np(V) humates are not changed due to the HA modification, which was found by the EXAFS measurements described in chapter 6.1.

Varying the pH of the studied system from pH 7 to pH 8, the LC of HA AHA as well as of AHA-PB increases as expected. However, the reduction of the LC due to the HA modification ($LC_{AHA} \rightarrow LC_{AHA\text{-}PB}$) is higher at pH 8 (65 %) than at pH 7 (35 %). That points to the fact that the influence of phenolic OH and other acidic OH groups on the Np(V) complexation by HA increases with increasing pH. This result can be attributed to a higher degree of deprotonated phenolic/acidic OH groups at pH 8 than at pH 7.

7 Studies on the influence of humic acids on the migration behavior of actinides

7.1 Effect of humic acid on the Th(IV) sorption onto quartz and quartz sand

The migration of tetravalent actinides in natural environments is influenced by several observable factors. Among these the sorption is one of the most important, which can be strongly affected by HA. The influence of HA on the sorption behavior of tetravalent actindes was exemplary studied for the Th(IV) sorption onto quartz and quartz sand.

The complexation of Th(IV) with humic substances [4,46,65-67] and the influence of humic or fulvic acids on Th(IV) sorption onto various minerals (especially amorphous silica or hematite) [68-72] has been described in the literature. In the present work the influence of HA on the Th(IV) sorption onto quartz and quartz sand was investigated by batch experiments in the pH range between pH 3 and pH 7.5.

7.1.1 Experimental

Materials

For the sorption experiments commercially available fine-grained quartz (100 % SiO_2, 63-200 µm) was applied (Merck). It was used without any pre-treatment. In addition to that we studied the Th(IV) sorption onto quartz sand (100–300 µm) of marine origin (Heerlen, Netherlands). Prior to its use the sand was washed with Milli-Q-water to remove soluble cations such as Na and K. Then it was annealed by 700 °C for 4 hours. After purification, the chemical composition of the sand was 0.3 % of Al, 0.02 % Ti, 0.02 % Fe, possibly illite, TiO_2, iron oxides, respectively, and 99.66 % SiO_2. In order to determine the fate of HA, ^{14}C-labeled synthetic HA type M42, charge M170 (cf. chapter 3.1) was used. For the preparation of the stock solutions (40 and 120 mg/L) HA was weighed, diluted with 0.1 M NaOH and filled to the required volume with 0.1 M $NaClO_4$ (pH 7). A Th(IV) stock solution of $5 \cdot 10^{-6}$ M ^{232}Th in 0.1M $HClO_4$ was prepared.

Sorption experiments

The sorption experiments were performed under inert gas conditions (N_2). 50 mg of mineral were weighed into 15 mL polypropylene (PP) centrifuge tubes (Nalgene). Then, 5mL 0.1 M $NaClO_4$ (pH 2.8) were added to the Merck-quartz. The samples were stirred for 30 minutes to remove adsorbed CO_2 from the mineral surface. Then, the pH values of the samples were adjusted between pH 3 and pH 7 by addition of $HClO_4$ or NaOH. For pre-equilibration the samples were continuously shaken and the pH values were controlled and readjusted over a period of 4 weeks. After pre-equilibration 5 mL 0.1 M $NaClO_4$ solution (pH 7) and 20 µL Th(IV) stock solution were added to the quartz suspension for the investigation of Th(IV) sorption onto Merck-quartz. The final concentration of Th(IV) in the solution was $1.2 \cdot 10^{-8}$ M. To determine the HA sorption onto quartz, 5 mL HA stock solution and 20 µL 0.1 M $NaClO_4$ solution (pH 7) were added to the quartz suspension. The final concentration of HA in the solution was 20 or 60 mg/L. For the investigation of the Th(IV) sorption onto Merck-quartz in the presence of HA, 5.02 mL pre-equilibrated Th(IV)-HA solution (equilibration time: 24 hours) of three different pH values (3.5, 5.0, 6.5) were added. The final concentrations of Th(IV) and HA in the solution were $1.2 \cdot 10^{-8}$ M and 20 mg/L, respectively. After addition of Th(IV), HA or Th(IV)/HA solutions, the pH values were readjusted immediately and after 1 day of contact time, if necessary. The samples were shaken for 4 days to reach the equilibration. After shak-

ing and short sedimentation of mineral particles, the supernatants of single samples were filtered using Minisart N membranes (Sartorius) with a pore size of 450 nm. Prior to filtering, the filters were rinsed with 1 mL of sample solution. The filtrates were analyzed for the final Th(IV) and HA concentration. The Th(IV) concentration in solution was determined by ICP-MS (Inductive Coupled Plasma-Mass Spectrometry, Mod. ELAN 500, Perkin Elmer) and the HA concentration in solution was measured by liquid scintillation counting (LSC, Beckman Instruments). Prior to the determination of the Th(IV) concentrations in the samples containing HA, HA was removed by digestion in a microwave in order to avoid any disturbing effects during ICP-MS measurements. The end pH values of the samples were determined in the remaining unfiltered solutions. Finally, the Th(IV) sorption onto vial walls was investigated. The vials were washed with water and dried. Then, 7 mL 1 M HNO_3 were added and the vials were shaken for 2 days. The Th(IV) concentration in the solutions was determined by ICP-MS. The amount of Th adsorbed on the mineral surface was calculated as the difference between the initial Th(IV) concentration ($1.2 \cdot 10^{-8}$ M) and the sum of the amounts of Th(IV) remaining in solution and Th adsorbed onto the vial walls. The same experiments were performed applying quartz sand as mineral phase.

In the experiments studying the Th(IV) sorption in the presence of HA, the solution of Th(IV) and HA was pre-equilibrated. After adding Th(IV) to HA solution, the pH was adjusted to 3.5, 5.0, and 6.5, respectively, and the solutions were equilibrated for 24 hours. To be sure, that there is no loss of Th(IV) due to colloid formation, the Th(IV) concentration in the solution of Th(IV) and HA was followed during the reaction time. It was found that the Th(IV) concentration in the solutions did not change.

In order to estimate the degree of Th(IV) sorption on filter materials, one series of direct measurements of Th(IV) in non-filtered supernatants was performed The results were compared with those from experiments with filtration. It could be shown that there was no significant difference between the concentration determined from the supernatant and the 450 nm filtrate in the pH range between pH 4.5 and pH 7.5.

7.1.2 Results and discussion

Th(IV) Sorption onto vial walls

Figure 7.1 shows the sorption of Th(IV) onto the walls of the PP vials in the absence and presence of HA. Depending on the pH, significant sorption of Th(IV) on PP tubes was observed for all experiments. The amount of Th(IV) sorbed onto the vial walls in the absence of HA increases with increasing pH to a maximum of 75 % at pH 7. From that it can be concluded that the Th(IV) sorption on the PP tubes competes with sorption on Merck-quartz. The presence of HA influences Th(IV) sorption on the walls. In comparison to the experiments without HA the percentage of Th(IV) sorbed onto the vial walls decreases to 15 %. The sorption of Th(IV) onto the walls is also influenced by the solid/solution ratio. An increase of the amount of Merck-quartz to 500 mg causes a decrease of the Th(IV) vial wall sorption of about 20 % in the acidic and about 10 % in the alkaline pH range, respectively. In the case of quartz sand comparable results were observed.

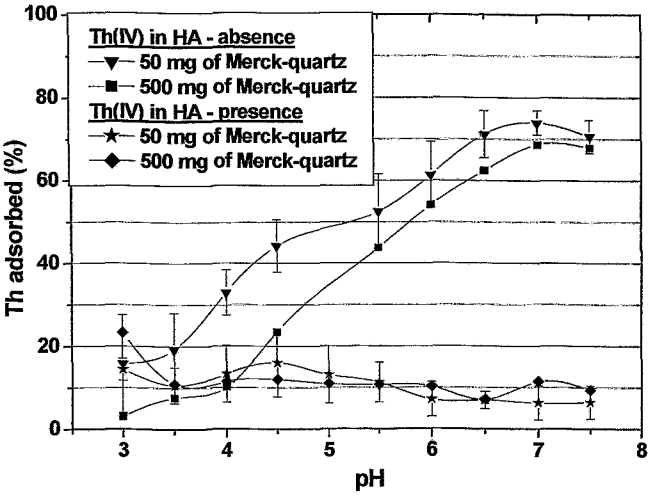

Fig. 7.1: Th(IV) sorption onto vial walls in the absence and presence of 20 mg/L HA.

HA sorption on Merck-quartz and quartz sand

Quartz sand has similar sorption properties as Merck-quartz. The observed sorption behavior of HA was almost the same for both of these materials (Fig.7.2). The sorption of HA on these minerals depends on pH. The HA sorption decreases with increasing pH value. The results show that about 80 % of HA are sorbed onto quartz at pH 3. However, there is a possibility

that a part of HA is precipitated at pH 3. There could be an overlapping of both processes, HA sorption and precipitation. At pH values ≥ pH 6 no HA adsorption was detected. These results correspond to the properties of quartz and HA in solution. Quartz has a low point of zero charge (PZC: 2.0 [73]), which results in predominantly negatively charged surface species ($>SiO^-$) in the pH range studied. At pH values > pH 6 carboxyl groups of HA are deprotonated, resulting in a negative charge of the HA. Due to electrostatic repulsion no HA is sorbed onto the negatively charged surface of quartz, which explains the observed sorption behavior. These results were confirmed in the experiments with higher concentration of HA (60 mg/L). The course of the sorption curve is identical. The sorption of HA decreases faster because of its higher concentration.

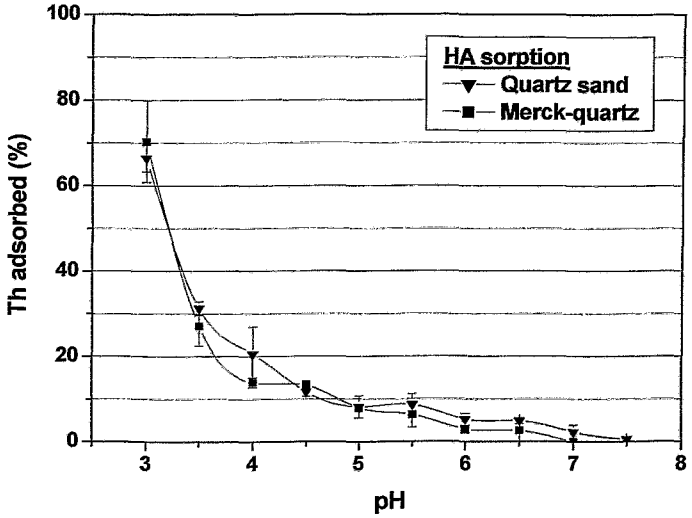

Fig. 7.2: HA uptake by Merck-quartz and quartz sand ([HA] = 20 mg/L).

Th sorption on Merck-quartz and quartz sand

The Th(IV) sorption onto Merck-quartz and natural quartz sand in the presence of HA was compared with the experiments performed under identical conditions, but in the absence of HA. In Fig. 7.3 the observed pH dependent Th(IV) uptake onto Merck-quartz in the absence and presence of synthetic HA HA type [^{14}C]M42 is shown. Figure 7.4 shows the sorption of Th(IV) onto quartz sand. The Th(IV) sorption onto Merck-quartz and also onto quartz sand is affected by the presence of HA. In the case of Merck-quartz the sorption curve can be divided into two parts. Between pH 4 and pH 4.5 the Th(IV) sorption in the presence of HA is slightly higher than in the HA free system. This small enhancement could be a result of the overcom-

pensation of the number of mineral binding sites blocked by sorbed HA. Additional binding sites for Th(IV) ions thus stem from HA itself. The Th(IV) uptake onto quartz in the presence of HA decreases with increasing pH value. This could be caused by the progressive desorption of HA from the quartz surface, leading to the complexation of Th(IV) in solution. Between pH 4.5 and pH 7.5 the Th(IV) sorption in the system without HA is low due to the high Th(IV) sorption onto the vial walls mentioned above which competes with the Th(IV) sorption on the quartz surface. Contrary to expectations, the Th(IV) sorption in the binary system is lower than in the system with HA. This can also be explained by the high wall sorption of Th(IV) in the absence of HA. Therefore, conclusions concerning the influence of HA on the Th(IV) sorption onto quartz at pH values > pH 4.5 are not possible.

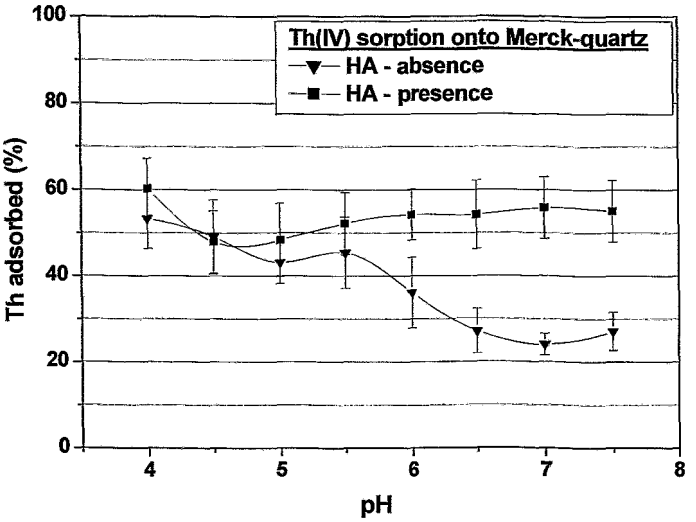

Fig. 7.3: Th(IV) uptake by Merck-quartz in the absence and presence of HA ($[Th^{4+}] = 1.2 \cdot 10^{-8}$ M, [HA] = 20 mg/L).

The sorption behavior of Th(IV) onto quartz sand in the presence of HA is comparable to that on Merck-quartz. However, in absence of HA, between pH 4 and 5.5, the sorption of Th(IV) onto quartz sand is significantly different compared to that on Merck-quartz in the same pH range (cf. Fig. 7.3). In this range a higher Th(IV) sorption onto quartz sand in the absence of HA was observed. There is one difference between these two investigated solids. Both materials differ in trace amounts of Fe, Al, Ti in form of oxides. So it seems probable, that these minor components occurring in quartz sand contribute to an enhanced Th(IV) uptake by forming additional binding sites. In contrast to that, the presence of HA slightly reduces the Th(IV) sorption onto quartz sand. The amount of Th(IV) sorbed onto quartz sand in the presence of

HA decreases with increasing pH value (pH 4 → pH 5). These observations can be due to the higher amount of dissolved HA in solution and the formation of Th(IV)-humate complexes. In the alkaline pH range the sorption of Th(IV) in the absence of HA is weak due to the high wall adsorption of Th(IV). Thus, it is not comparable with the sorption in the presence of HA.

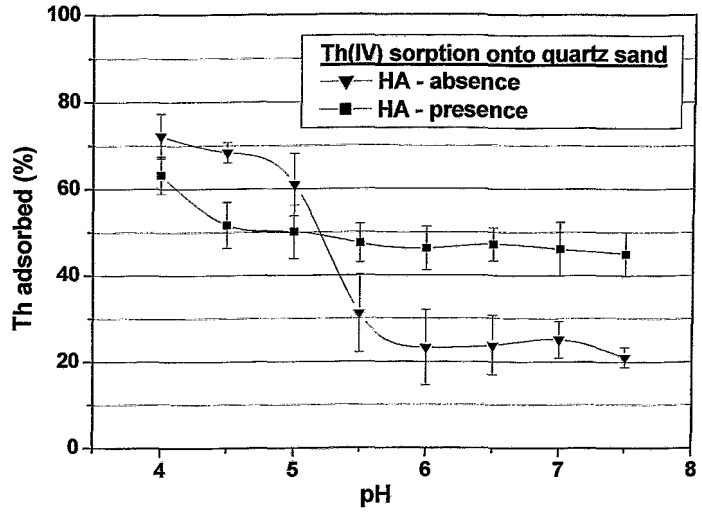

Fig. 7.4: Th(IV) uptake by quartz sand in the absence and presence of HA ([Th(IV)] = $1.2 \cdot 10^{-8}$ M, [HA] = 20 mg/L).

Th(IV) and HA type [^{14}C]M42 show a pH-dependent sorption behavior onto Merck-quartz and natural quartz sand. The sorption of Th(IV) is slightly affected by HA. The influence of HA on the Th(IV) sorption depends on the pH and the mineral phase.

7.2 Neptunium(V) sorption onto granite in the absence and presence of humic acid

In Germany, besides salt formations also granitic subsurface environments are taken into account as potential host formations for the geological disposal of radioactive waste [74]. For this study, granite from Eibenstock was chosen which determines as geologic formation a large area of the former uranium mining areas in the Western Erzgebirge in Saxony, Germany. It was already applied for uranium(VI) sorption studies [75]. Granite is mainly composed of the minerals quartz, orthoclase, biotite, albite, and muscovite.

In this work, the sorption of Np(V) onto granite and its main mineral constituents is studied under anaerobic conditions at an ionic strength of 0.1 M as a function of pH in a series of

batch equilibrium experiments. Furthermore, the effect of HA on the Np sorption is studied in order to determine whether humic material is likely to significantly influence Np sorption on granite.

7.2.1 Experimental

Materials

The rock material granite, collected in the region Eibenstock (Germany), is composed of 45 vol.% quartz (SiO_2), 35 vol.% orthoclase ($KAlSi_3O_8$), 7.5 vol.% biotite ($K(Mg,Fe^{2+},Mn)_3[(OH,F)_2/(Al,Fe^{3+})Si_3O_{10}]$), 7.5 vol.% albite ($NaAlSi_3O_8$), 4 vol.% muscovite ($KAl_2[(OH,F)_2/AlSi_3O_{10}$), and 1 vol.% opaque minerals. The 63 to 200 µm grain size fractions of the solids were applied for sorption experiments. The Np(V) stock solutions were obtained by dissolving solid $^{237}NpO_2NO_3$ in 0.1 M HNO_3. As HA the ^{14}C-labeled synthetic HA type M42 (batch M170, chapter 3.1) was used for the experiments.

Sorption experiments

For sample preparation, all solutions were prepared with CO_2-free water in a nitrogen atmosphere glovebox. 5 mL of a 0.1 M $NaClO_4$ solution (pH 2.8) were added to 50 mg of the geomaterial in 15 mL vials (PP, Nalgene). The samples were stirred for 30 min to remove adsorbed CO_2 from the mineral surface. After that, the desired pH value (pH 4 to pH 11) was adjusted by addition of diluted $HClO_4$ or carbonate-free NaOH. During pre-equilibration of the samples (about 4 weeks), the samples were shaken continuously and the pH values were readjusted until they were stable. The sorption experiments in the absence and presence of HA were started by adding 5 mL 0.1 M $NaClO_4$ solution (pH about 7) and 5 mL HA stock solution (^{14}C-M42, 0.1 M $NaClO_4$), respectively, and about 80 µL of the Np(V) stock solution simultaneously to the preconditioned minerals. The Np(V) stock solutions were prepared prior to each sorption step by separating ^{233}Pa from ^{237}Np using Dowex-50. The oxidation state of the Np in the stock solutions was spectroscopically confirmed to be pentavalent. The final Np and HA concentration in the sample solutions was 1.3×10^{-6} M and 27 mg/L, respectively. The solid solution ratio was 50 mg/10 mL. The pH was readjusted immediately after addition of the stock solutions. Then, the samples were shaken at room temperature for about 160 hours during which the Np and HA sorption onto the solids reached equilibrium. After centrifuga-

tion of the samples (3500 rpm, 15 min), the equilibrium pH values were recorded. Subsequently, the supernatant was filtered (450 nm, Minisart RC 15, Sartorius). Prior to filtering, the filters were rinsed with 1 mL of the sample solutions.

In the filtrates the final Np and HA concentration was determined by liquid scintillation counting (Beckman Instruments) using α/β-discrimination. For this, 1 mL of the filtrate was mixed with 5 mL of a Ultima Gold scintillation cocktail. The amount of Np and HA adsorbed to the mineral surface was calculated as the difference between the initial Np and HA concentrations and the final Np and HA concentrations in the 450 nm filtrates.

7.2.2 Results and discussion

The Np sorption in the absence of HA and the Np and HA sorption in experiments performed in the presence of HA is shown for granite and its mineral constituents muscovite, orthoclase, albite, quartz, and biotite in Fig. 7.5.

The sorption experiments, carried out in the absence of HA, show that the Np sorption starts between pH 7 and pH 8 and increases with increasing pH value.

For the sorption experiments performed in the presence of HA the following results were obtained. As expected, the HA sorption decreases with increasing pH value. The reason for the sudden increase of the HA sorption onto biotite between pH 9.2 and pH 11 is not known. Compared to the Np sorption in the absence of HA, the Np sorption onto granite is decreased by HA between pH 7 and pH 11. The Np sorption onto muscovite and orthoclase is somewhat increased by HA between pH 6 and pH 9 and at higher pH values relatively strongly decreased. The Np sorption onto albite and quartz is not changed by HA up to pH 10 and pH 9, respectively. At higher pH values it is again relatively strongly decreased. In case of biotite, the Np sorption is decreased by HA between pH 7 and pH 11, as was found also for granite.

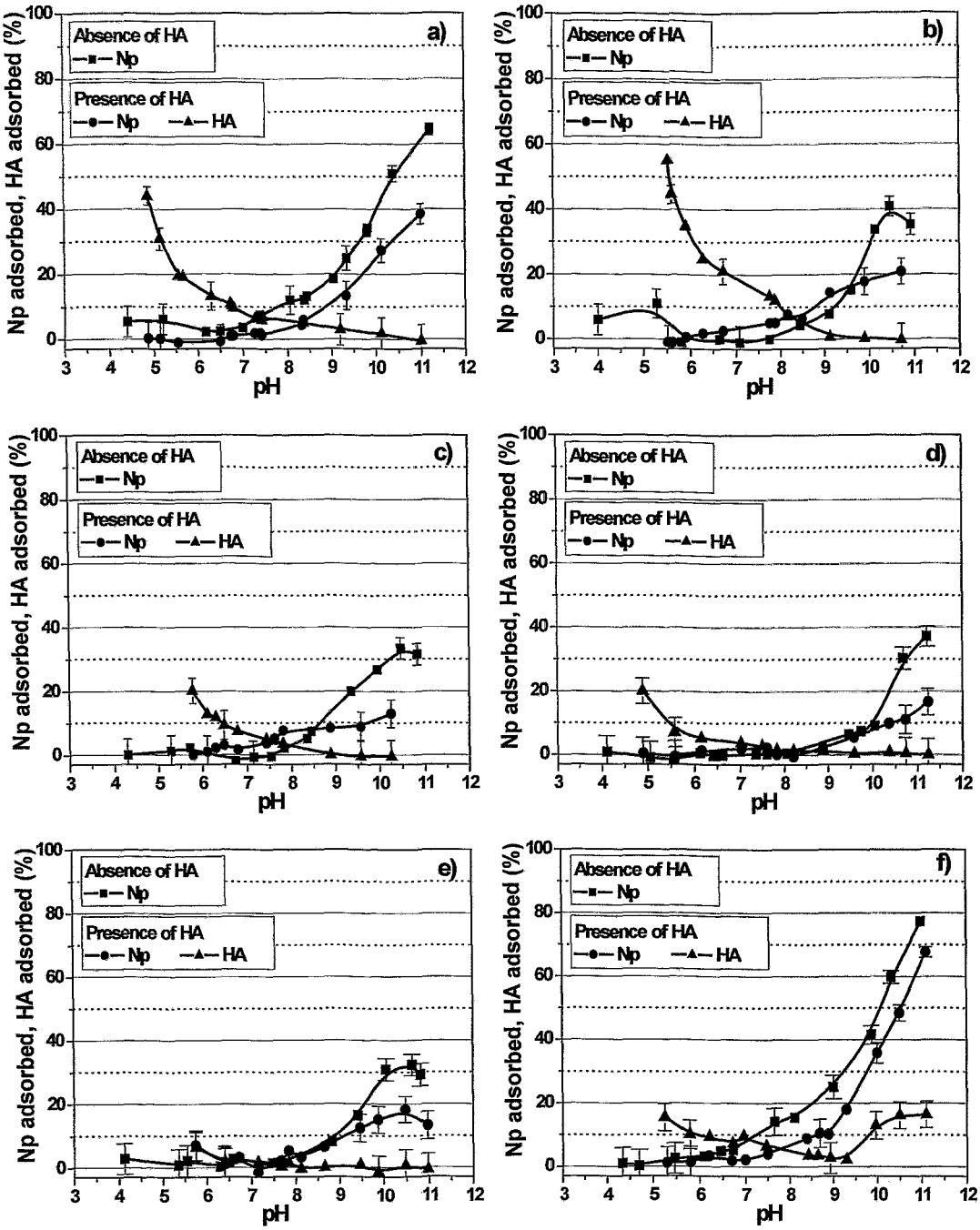

Fig. 7.5: Np and HA uptake by (a) granite, (b) muscovite, (c) orthoclase, (d) albite, (e) quartz, and (f) biotite ($[NpO_2^+] = 1.3\times10^{-6}$ M; [HA] = 27 mg/L; I = 0.1 M $NaClO_4$; CO_2-free).

The Np speciation for the experimental conditions applied in this study is shown in Fig. 7.6. It was calculated with the geochemical computer code EQ3/6 [12] applying the Np(V) hydrolysis constants compiled in the NEA data base [61], the neptunyl humate complexation constant

log β = 3.6 and the pH function of the loading capacity (LC) with LC = -0.589 + 0.101 · pH (cf. Fig. 8.1 in chapter 8). The results show that the free neptunyl ion predominates the Np speciation in aqueous solution. The Np(V) hydrolysis species in solution ($NpO_2OH_{(aq)}$) is increasingly formed between pH 9.5 and pH 11. In the presence of HA, $NpO_2HA(I)$ is formed between pH 6 and pH 11 with a maximum of 13.6 % at about pH 10.5. For the pH region higher than 9, the formation of the mixed complex $[NpO_2(OH)HA]_{coll.}$ is suggested by Marquardt et al. [63]. Presently, this complex cannot be quantified thermodynamically, however, this complex would explain the strong reduction of the Np sorption by HA at pH values higher than 9 and 10, respectively.

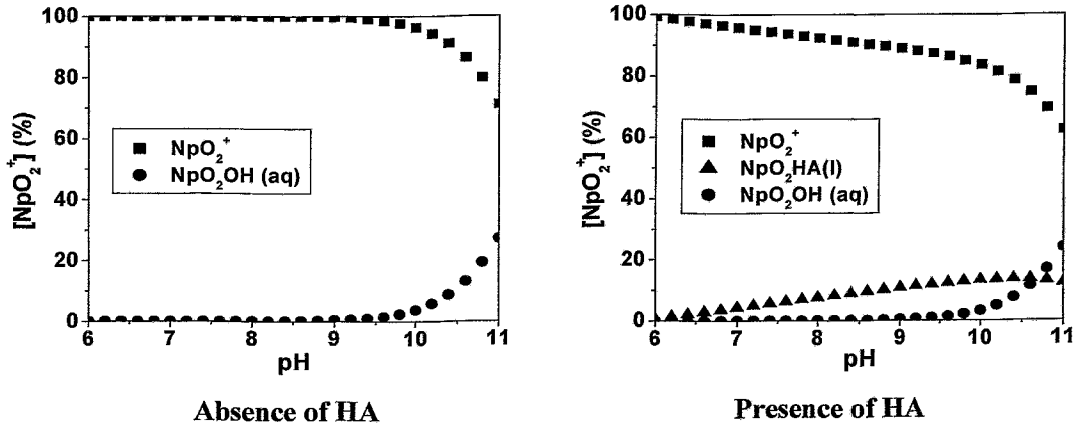

Fig. 7.6: Np speciation in solution
($[NpO_2^+] = 1.3\times10^{-6}$ M; [HA] = 27 mg/L; I = 0.1 M $NaClO_4$; CO_2-free).

The results in Fig. 7.5 have shown, that both granite and biotite show a strong Np sorption in the alkaline pH region. Furthermore, compared to the Np sorption experiments in the absence of HA, the reduction of the Np sorption by HA between pH 7 and pH 11 is similar for both materials. From this, it is concluded that biotite is the dominating mineral phase in the rock material granite for the Np sorption.

Mössbauer spectroscopic measurements have shown that in un-weathered biotite 84.5 % of Fe_{total} occur as Fe(II) [76]. This Fe(II) occurring in biotite and thus, also in granite could possibly lead to a reduction of Np(V) to Np(IV). For magnetite it was found by Nakata et al. [77] that Np(V) is reduced to Np(IV) by Fe(II) on the surface of magnetite but not by Fe(II) ions released from magnetite into solution. Such a reduction of Np(V) to Np(IV) on the mineral surface would lead to an increase of the Np sorption. However, for Np sorption experiments in the presence of HA it was found by Zeh et al. [78] that especially the combination of Fe(II)

and HA could lead to a reduction of Np(V) to Np(IV). Compared to Np(V), Np(IV) is generally stronger complexed by HA due to its higher charge [79]. Thus, the Np sorption onto granite and biotite would be reduced compared to experiments without HA. The oxidation state of Np in the supernatant solutions of the sorption samples without and with HA was checked by liquid-liquid extraction using TTA. So far, no Np(IV) could be detected in solution.

7.3 Study of the influence of humic acids on the migration of uranium(IV)/(VI) in quartz sand

The influence of HA on the migration of actinides in the environment can be studied in laboratory column experiments. Column experiments with natural sand and groundwater systems rich in humic substances demonstrated that a certain fraction of the load actinides (e.g., U(VI) [80], Am(III) [81] and Np(IV)/(V) [82]) migrate humic colloid-borne as fast as the groundwater flow. This colloid-borne migration is controlled by kinetic processes.

The present study focuses on the influence of HA on the migration of U(VI) and U(IV) in a quartz sand system at a laboratory scale. The migration of U(VI) was studied in the presence and absence of HA. In addition to that, the HA migration under the applied experimental conditions was described. In order to characterize the migration behavior of U under reducing conditions we studied the migration of the redox couple U(IV)/(VI) in the presence of HA.

7.3.1 Experimental

Experimental set-up

Migration experiments were performed in a glove box under nitrogen atmosphere. The experimental set-up is shown in Fig. 7.7.

Columns 250 mm in length and 50 mm in diameter, tightly packed with quartz sand were used. A marine fine sand, Gaussian distributed in particle size, with a mean grain diameter of 153 µm from Heerlen, Netherlands, was chosen for its chemical purity (see chapter 7.1.1). Prior to use the quartz sand was washed with Milli-Q water and annealed for 6 hours at 700 °C. After packing, the sand columns were equilibrated with degassed $NaClO_4$ solution (0.1 M, pH 7.5) over a period of 3 weeks.

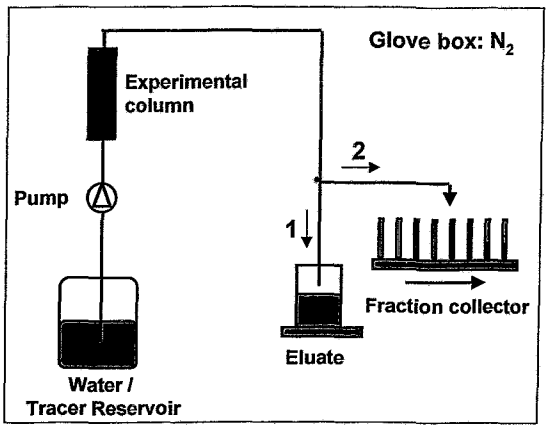

Fig. 7.7: Set-up of the column experiments.

All experiments were carried out at room temperature under absence of light, applying degassed solutions. Continuous pulse injection was applied. The tracer impulse was followed by a multiple elution of the column with 0.1 M $NaClO_4$ (pH 7.5). For the determination of the hydraulic and transport parameters of the columns, tritiated water (HTO) was used as conservative tracer. Each experimental problem was studied in a separate column in order to avoid mutual interferences. The transport parameters and the experimental conditions for all experiments are listed in Tab. 7.1. It shows a good reproducibility of the column packing.

Tab. 7.1: Experimental conditions and transport parameters of the column experiments.

Exp.	Impulse (mL)	HA (mg/L)	U (mol/L)	Darcy velocity (m/s)	Effective pore volume (mL)	Dispersion coefficient (m^2/s)
1	660	49.9	-	$3.3 \cdot 10^{-6}$	181	$5.5 \cdot 10^{-5}$
2	716	50.3	-	$4.4 \cdot 10^{-6}$	181	$5.5 \cdot 10^{-5}$
3	690	-	$1.1 \cdot 10^{-5}$	$3.4 \cdot 10^{-6}$	181	$6.0 \cdot 10^{-5}$
4	457	49.9	$1.0 \cdot 10^{-5}$	$3.3 \cdot 10^{-6}$	178	$6.1 \cdot 10^{-5}$
5	462	50.0	$1.0 \cdot 10^{-6}$	$3.6 \cdot 10^{-6}$	173	$5.0 \cdot 10^{-5}$

Humic acid migration

The HA migration in the quartz sand system in the presence and absence of U was studied applying synthetic HA type M42 (cf. chapter 3.1). It shows functional and structural properties that are comparable to natural HA. In addition to that, synthetic HA type M42 exhibits a U(VI) complexation behavior that is comparable to natural HA [83]. In order to perform a very precise HA detection in environmentally relevant concentrations we spiked the HA solutions with ^{14}C-labeled synthetic HA type M42 (batch M170, 2.38 MBq/g, cf. chapter 3.1).

For the study of the HA migration in the absence of U (experiments 1 and 2), HA solutions with a concentration of 50 mg/L (specific activity: 70 kBq/L) were prepared by dissolving unlabeled and ^{14}C-labeled synthetic HA type M42 in 0.1 M $NaClO_4$ solution. The pH values of these solution were adjusted to pH 7.5 using dilute $HClO_4$ and NaOH solution.

Uranium(VI) migration in absence and presence of humic acid

The U(VI) migration in the absence of HA (experiment 3) was studied applying a $1.1 \cdot 10^{-5}$ M $UO_2(ClO_4)_2$ (0.1 M $NaClO_4$, pH 7.5) solution.

An acidic $UO_2(ClO_4)_2$ solution was added to a ^{14}C-labeled HA solution in order to determine the U(VI) migration in the presence of HA (experiment 4). The final uranyl humate solution with a HA concentration of 50 mg/L (^{14}C: 70 kBq/L) and an U concentration of $1.0 \cdot 10^{-5}$ M (0.1 M $NaClO_4$) was spiked with 40 kBq/L ^{234}U containing traces of ^{232}U. Before the injection into the column this solution was equilibrated for 98 hours.

Uranium(IV) migration in presence of HA

For the study of the U(IV) migration in the presence of HA (experiment 5), the U(IV) was prepared by electrochemical reduction of an acidic uranyl (^{234}U) nitrate solution. The absence of U(VI) in the U(IV) stock solution was confirmed by time-resolved laser-induced fluorescence spectroscopy. For experiment 5, the acidic $^{234}U(IV)$ solution was added to a ^{14}C-labeled HA solution. The final concentrations of the uranium humate solution (0.1 M $NaClO_4$, pH 7.5) amounted to 50 mg/L HA (^{14}C: 70 kBq/L) and $1.0 \cdot 10^{-6}$ M ^{234}U (60 kBq/L). This solution was equilibrated for 2 hours prior to start of the experiment.

In order to differentiate between U(IV) and U(VI) redox speciation was determined by liquid-liquid extraction using TTA (thenoyltrifluoracetone; Fluka,) [84]. The extraction yield was found to be 90 %. The standard deviation amounts to 5 %.

Measurement of breakthrough curves

Breakthrough curves of HTO, HA and U were measured by fraction analysis using liquid scintillation counting (LSC, Beckman Instruments) for HTO, ^{14}C and ^{234}U, and ICP-MS for ^{238}U. The LSC spectra were deconvoluted to determine the activity contribution of ^{232}U daughter nuclides.

Analysis of the solids

After the end of column experiments 4 and 5 samples of the filling materials were taken at distances of about 10 mm, 125 mm, and 240 mm from the inlet. 3 g of the sample material were shaken with 1 M NaOH and 1 HNO_3, respectively, for three days in order to elute the adsorbed amount of ^{14}C and ^{234}U. The supernatant solutions were analyzed using LSC as described above.

Data processing and evaluation

For depicting the breakthrough curves all effluent concentrations were normalized to the input concentration c_0 of the tracer solution. The time axis (abscissa) is represented as the ratio of effluent pore volume and effective pore volume, determined from HTO breakthrough. The measured breakthrough curves were evaluated by means of the one-dimensional transport equation [85]. Assuming steady-state flow in a homogeneous matrix, linear sorption, and a first-order decay it may be written as

$$R_f \frac{\partial c}{\partial t} = D \frac{\partial^2 c}{\partial x^2} - v \frac{\partial c}{\partial x} - \mu c \qquad (7.1)$$

where c is the concentration, v is the average pore-water velocity, D is the hydrodynamic dispersion coefficient, μ is a first order decay coefficient, R_f is the retardation factor, x is distance, and t is time. The retardation factor may be determined from the ratio of effluent pore volume at tracer breakthrough (V) and the effective pore volume (V_P)

$$R_f = \frac{V}{V_P} \qquad (7.2)$$

and is related to the empirical distribution coefficient K_D by

$$R_f = 1 + \frac{\rho K_D}{\varepsilon} \qquad (7.3)$$

where ρ is the bulk density of the porous medium and ε is the effective porosity. Retardation factors exceeding unity indicate a retarded transport compared to a conservative tracer, whereas values less than unity refer to an accelerated transport. The last term of the right hand side of Eq. (7.1) is a sink term that describes the deposition flux of colloidal particles, also referred to as filtration [86]. The parameter μ may be interpreted as deposition rate coefficient.

The CXTFIT code [85] was utilized to estimate the parameters v, D, and μ from the break through curves using a nonlinear least-square optimization. The standard errors of the simul-

taneously fitted parameters were derived from the sum of squared residuals between the observed and the fitted concentrations.

The tracer recovery in the eluate R_{eluate} was approximated by numerical integration of the breakthrough curve applying the trapezoidal rule and normalization to the input quantity.

7.3.2 Results and discussion

Speciation of uranium

The interpretation of the experimental data requires detailed knowledge on the species distribution. In a 10^{-5} M carbonate free U(VI) solution at pH 7.5 the dominating U(VI) species is $UO_2(OH)_2(aq)$. In presence of HA about 90 % of U(VI) are complexed in form of a ternary U(VI) humate complex ($UO_2(OH)HA(I)$). At a redox potential of 50 mV the U speciation in carbonate free 10^{-6} M U solution is dominated by 84 % of $UO_2(OH)_2(aq)$ as shown in Fig. 7.8.

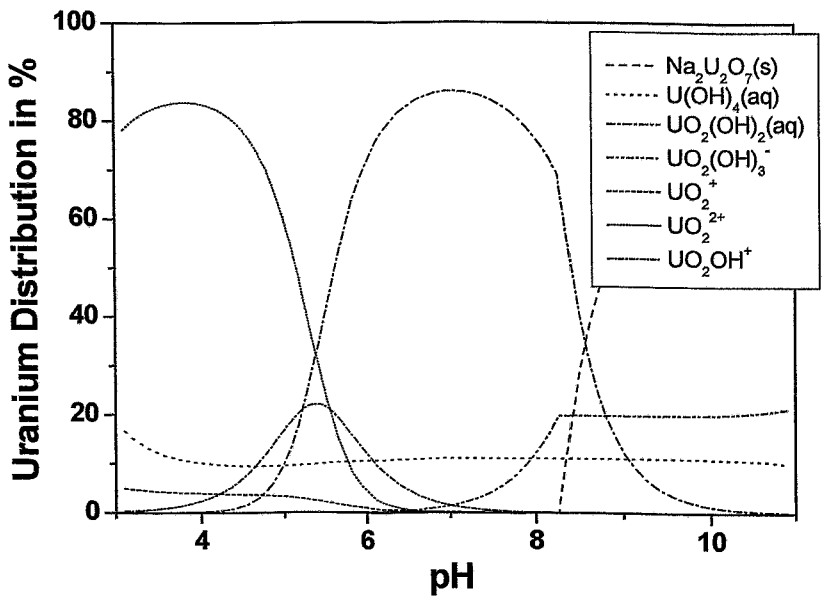

Fig. 7.8: Speciation of uranium at a redox potential of 50 mV (Thermodynamic data taken from [87]).

In addition, amounts of 11 % $U(OH)_4(aq)$ and 4 % $UO_2(OH)_3^-$ occur. No species calculations in presence of HA are possible due to the lack of thermodynamic data for the U(IV) HA complexation.

In the studied system HA type M42 controls the redox potential. A redox potential of about 50 mV can be derived for the studied system.

Humic acid migration in absence of uranium (Experiments 1 and 2)

Evaluating the HA breakthrough curves as shown in Fig. 7.9, the retardation factor R_f as well as the eluate recovery on HA were determined (Tab. 7.2). The R_f values indicate an only slightly retarded transport of the HA compared to HTO (R_f: 1). Thus, there are no significant interactions between HA and the quartz sand surface, due to the negative charge of both species at pH 7.5. Batch experiments confirm this result. The detected R_f implies that there are no grain size exclusion effects which would be reflected in R_f values smaller than 1. The HA recovery of about 0.9 points to irreversible immobilization processes, e.g., filtration effects. The according filtration coefficient μ in Eq. (7.1) amounts to $(4.0 \pm 0.2) \cdot 10^{-6}\ s^{-1}$.

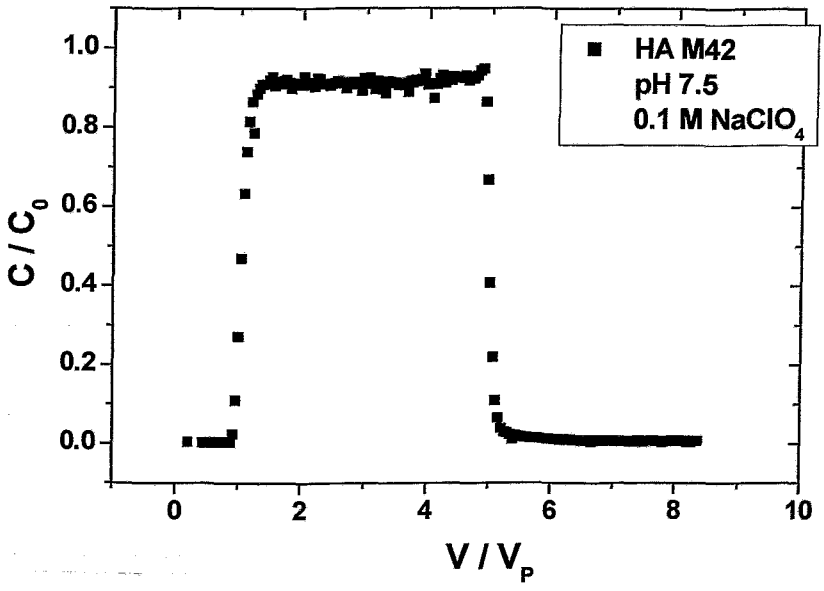

Fig. 7.9: Breakthrough curve of HA M42 in experiment 2. C: measured and C_0: initial concentration; V: effluent volume; V_P: effective pore volume.

Tab. 7.2: Retardation factors, R_f, and eluate recoveries, R_{eluate}, of the injected species.

Exp.	Species	R_f	R_{eluate}
1	HA	1.02 ± 0.02	0.91 ± 0.01
2	HA	1.02 ± 0.02	0.92 ± 0.01
3	U(VI)	2.09 ± 0.10	0.43 ± 0.02
4	HA	1.05 ± 0.02	0.85 ± 0.01
4	U(VI)+HA	1.19 ± 0.02	0.80 ± 0.01
5	HA	1.04 ± 0.02	0.90 ± 0.01
5	U(VI)+HA	1.11 ± 0.02	0.90 ± 0.06
5	U(IV)+HA	1.07 ± 0.02	0.66 ± 0.05

Uranium(VI) migration in absence of HA (Experiment 3)

The U(VI) migration in absence of HA is characterized by a strong retardation which is reflected in the R_f value greater than 1 (cf. Tab. 7.2 and Fig. 7.10). The shape of the breakthrough curve indicates kinetically controlled processes [85]. Especially the observed tailing directs to a slow release of U(VI) from the quartz surface even after five eluted pore volumes. The low U(VI) recovery can be caused by precipitation or sorption processes. At a 10^{-5} M U(VI) concentration the solid phase schoepite ($UO_3 \cdot 2H_2O$) is saturated. However, it is not expected that this solid is formed during the residence time of U in the system.

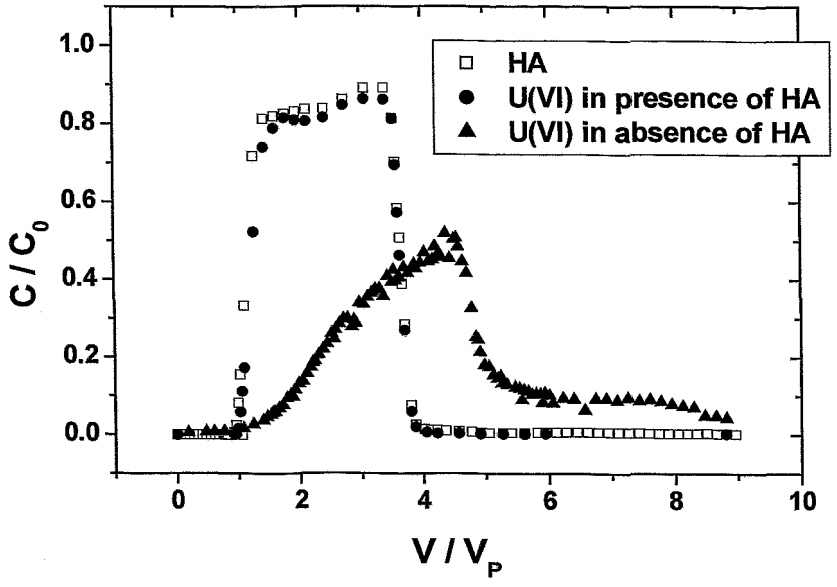

Fig. 7.10: Breakthrough curves of HA and U(VI) in experiments 3 and 4. C: measured and C_0: initial concentration; V: effluent volume; V_P: effective pore volume.

U(VI) migration in presence of HA (Experiment 4)

HA bound U(VI) exhibits a completely different breakthrough behavior which is depicted in Figure 7.10. In presence of HA the U(VI) transport is accelerated and the U(VI) recovery is increased. This behavior is attributed to the formation of soluble U(VI) humate complexes. However, for both components, HA and U(VI), slightly different R_f values and recoveries were detected (cf. Tab. 7.2). These effects are caused by association/dissociation processes in the system HA-U(VI)-quartz. A certain part of U(VI) dissociates from the soluble humate complex and adsorbs onto the quartz surface. Comparing differences in the recoveries of U(VI) and HA one can conclude that about 5 % of U(VI) is irreversibly bound on the quartz

surface. Considering the results reported by Artinger et al. [80], it can be assumed that these processes are kinetically controlled.

Migration of the U(IV)/U(VI) couple in presence of HA (Experiment 5)

The distribution of U(IV) and U(VI) in the starting solution amounts to 8 % and 92 %, respectively. This is comparable to the calculated redox species distribution at 50 mV mentioned above. This redox speciation was stable over the duration of the experiment. Moreover, this initial ratio of U(IV) and U(VI) was also found in the effluent solutions. This indicates that no oxidation processes occur in the column.

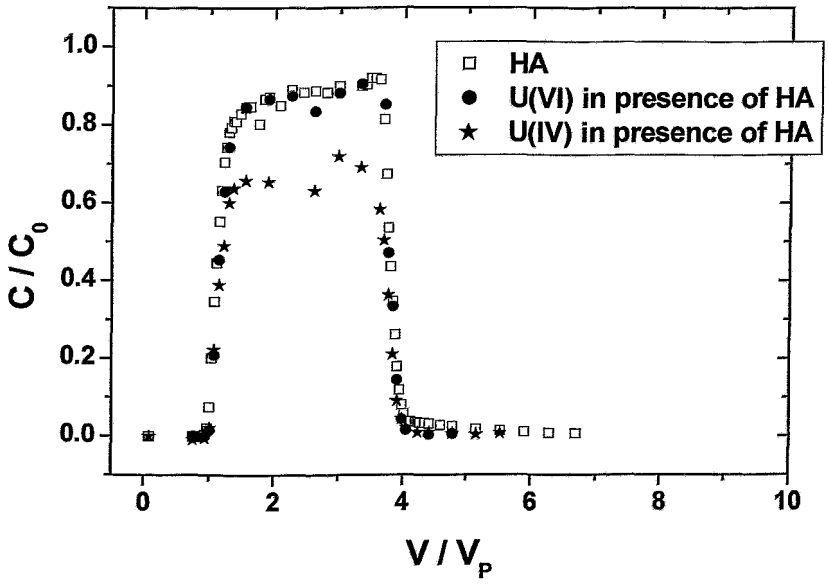

Fig. 7.11: Breakthrough curves of HA, U(IV), and U(VI) in experiment 5. C: measured and C_0: initial concentration; V: effluent volume; V_P: effective pore volume.

Figure 7.11 shows the breakthrough curves for HA, U(IV) and U(VI). Based on them R_f values and eluate recoveries listed in Tab. 7.2 are derived. As with the case of U(IV), the association/dissociation processes mentioned above control the transport behavior in presence of HA ($R_f > 1$). Although U(IV) and U(VI) are characterized by different thermodynamic properties [88] no significant differences in their R_f values were observed under the applied experimental conditions.

A comparison of the U balances in experiments 4 and 5 shows that a decreased total U concentration results in a slightly higher recovery. In experiment 5 the total recoveries of both, U(VI) and HA, agree very well. This fact refers to a HA bound U(VI) transport.
In spite of the increased uncertainty of the extraction data, the U(IV) recovery is lower than that of U(VI). This points to a stronger interaction of U(IV) with the quartz sand surface and thus a more distinct immobilization. Nevertheless, there are strong indications that HA has a mobilizing effect on the U(IV) transport in the investigated system due to its complexing ability.

Balances of the reactive tracers

In addition to the eluate recoveries the adsorbed amounts of the tracers are investigated. Figure 7.12 shows the spatial distribution of ^{14}C and ^{234}U within column 4 and 5.

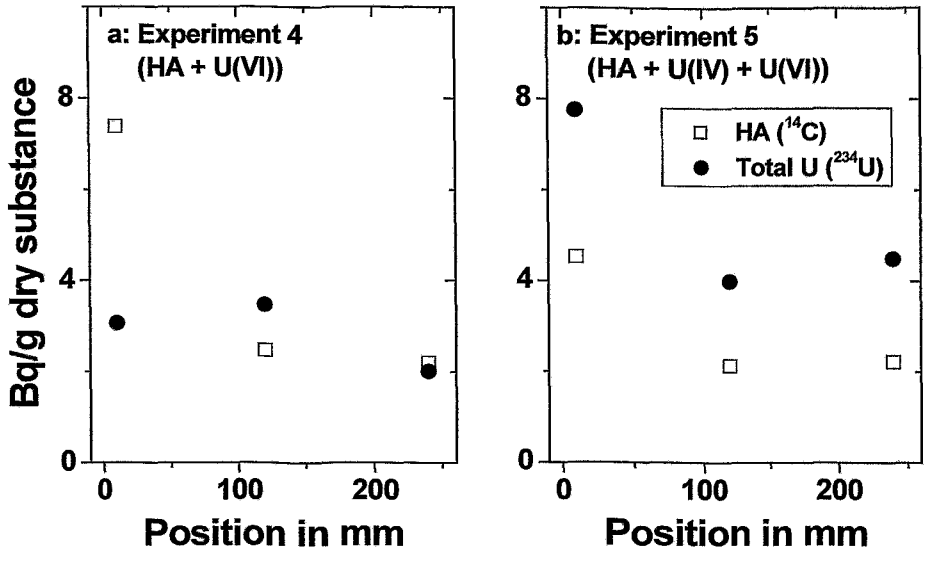

Fig. 7.12: Spatial distribution of ^{14}C and ^{234}U within column 4 and 5.

The amount of ^{234}U represents the total activity of U. U(IV) and U(VI) are not to be distinguished after contact with air and HNO_3 extraction. The curves suggest a close relation between both tracers with exception of the U concentration near the column inlet of experiment 4. Possibly this single measurement is not representative.

Tab. 7.3: Balances of reactive tracers in experiment 4 and 5.

Recovery	Experiment 4		Experiment 5	
	Humic acid (^{14}C)	Uranium (^{234}U)	Humic acid (^{14}C)	Uranium (^{234}U)
R_{eluate}	0.85 ± 0.01	0.80 ± 0.01	0.90 ± 0.01	0.82 ± 0.01
R_{solid}	0.11 ± 0.003	0.06 ± 0.002	0.07 ± 0.002	0.15 ± 0.004
R_{total}	0.96 ± 0.01	0.86 ± 0.01	0.97 ± 0.01	0.97 ± 0.01

The total balance of the reactive tracers in experiment 4 and 5 are summarized in Tab. 7.3. With exception of ^{234}U in experiment 4 the total recoveries are close to unity. Thus container walls do not adsorb significant amounts of tracer. The balances support the conclusions drawn from recoveries, in particular the close relation between the migration of HA and U.

From these experiments it can be concluded that HA affects the migration behavior of both U(IV) and U(VI). In presence of HA U(VI) is significantly mobilized. A similar effect is supposed for U(IV). Both U redox species exhibit a different migration behavior, in particular reflected in their effluent balances.

The system under investigation represents a strong simplification of natural aquifers in view of geology and solution composition. More complex compositions are typical in natural aquifer systems. Strong reducing conditions can occur in deep groundwaters. There, the tetravalent actinides become more important. However, the performed experiments are suitable in order to identify sensitive relationships between actinides, HA and rock matrix and to establish more sophisticated concepts for understanding and modeling of complex migration processes.

8 Integration of the Metal Ion Charge Neutralization Model into the geochemical speciation code EQ3/6

There are many different models used to describe interactions between humics and actinides. The most prominent ones can be categorized into two major groups. They differ in their approaches to describe the binding places at the humics molecule:

A) Discrete binding places

- Metal Ion Charge Neutralization [11]
- Model VI [89]

- Polyelectrolyte Model [90]

B) Continuous distribution function(s)

- NICA-Donnan model [91]
- CONICA model [92]

During this project, the metal ion charge neutralization (MICN) model was favoured due to its relative simplicity and the few parameters required. Moreover, there is ample experience and experimental data records available for this model in the project team.

One essential parameters required by the model is the proton exchange capacity (PEC). A normalization to multiple charged metal ions then gives a metal-specific total of the available binding sites. The next parameter, the loading capacity (LC) describes that part of the binding sites actually accessible for ligands (again normalized to the charge of the ligand). LC is a phenomenological parameter and thus a function of pH, ionic strength, ligand and others.

One of the tasks of the project was the embedding of the MICN into an existing geochemical speciation code. This should allow for a fast and easy computation of complex speciation patterns in real systems. Relying on an already established software ensures that algorithms and implementation is counter-checked, thus computations are reproducible and reliable. Furthermore, such software can take advantage from comprehensive pre-compiled standard databases. The software of choice was the EQ3/6 [12] geochemical speciation package well suited for thermodynamic and kinetic modeling of complex and heterogeneous systems. It was developed by Thomas J. Wolery from the Lawrence Livermore National Laboratory. All following work was based on the code version 7.2b of August 18, 1995. EQ3/6 is able to handle all reactions in aqueous solution, including redox reactions, it considers precipitation and dissolution of pure mineral phases and solid solutions, and has also kinetic modules to compute reaction paths. EQ3/6 is programmed in FORTRAN 77 (ANSI), there are both UNIX and PC versions, and an exhaustive manual is provided. Very important is the certification by the U.S. DoE as part of the Yucca Mountain Project. Several databases are included in the package.

But so far the EQ3/6 software does not consider any humics-metal interactions, despite that such interaction can not be neglected in many natural systems. Therefore, the MICN approach has been integrated into EQ3/6. This required changes in Fortran code of the modules for the

data input, the addition of the computation of LC as f(pH) and the determination of the metal complex concentration. The program was compiled both as UNIX version (f77 compiler) and MS Windows NT version (Lahey LF 90 compiler). A major goal of the development was to reach a flexible solution with minimum impact on the existing input file and database structure. So unused options in the EQ3/6 input files now trigger functions such as the mode of the humics hydrolysis (see below), or the type of the pH function of LC. The data input processing is performed in a separate shell script module, allowing for the computation of LC as a function of pH or ionic strength and of the metal-specific concentration of available binding sites at the humic matter. These scripts enable semi-automatic parameter scans substantially increasing computation speed.

Humics species were included into the EQ3/6 thermodynamic database by defining pseudo-species based on fictitious elements because the very nature of humics prevents an exact stoichiometry and formation reaction based on simpler organic molecules. The humics species set exists twice: one version is based on a formally uncharged humics molecule Hx(aq), the other one (HhH_2) considers two deprotonation steps. An input option allows the switch between these two alternative formulations. Examples for the two alternative (and mutually exclusive) formulations are given below:

a) reactions for humic acids without protolysis (standard)

- basis species **Hx(aq)** (formally uncharged)
- reactants **UO2Hx++, UHx++++, UO2HxOH+, NpO2Hx+, ..**

b) reactions for humic acids including protolysis

- basis species **HhH2(aq)** (formally uncharged)
- reactants **Hh-, Hh--, UO2Hh, ...**

Using input option switches certain species can be blocked or the log β of their formation reaction can be modified, independent form the standard database used.

A verification of the changed EQ3/6 version was done through speciation modeling of the systems U(VI)-HA and Np(V)-HA. In a first step published LC values for the HA-actinide system were fitted to a linear function as the simplest possible approach. Figure 8.1 shows the results for Np(V).

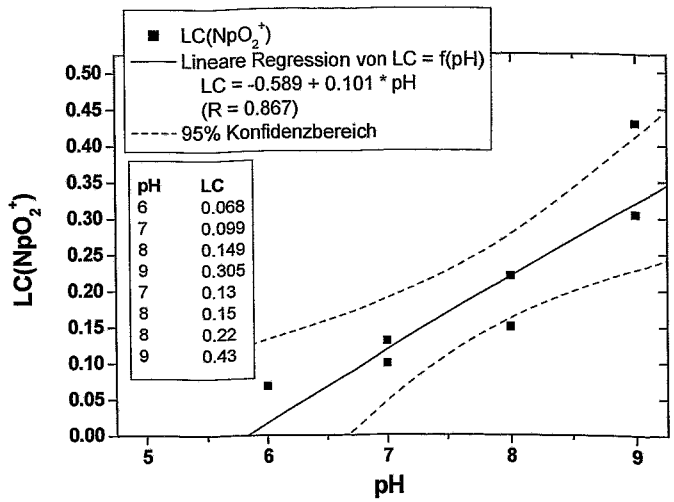

Fig. 8.1: Loading capacity $LC(NpO_2^+)$ as function of pH.

Then the obtained pH-LC relationship was used to compute the actinide speciation pattern as given in Fig. 8.2, again for Np(V). The experimental conditions are as follows: 100 mg/L HA, $2 \cdot 10^{-5}$ M NpO_2^+, 0.1 M $NaClO_4$, in air, log $\beta = 3.6$ for the formation of the complex.

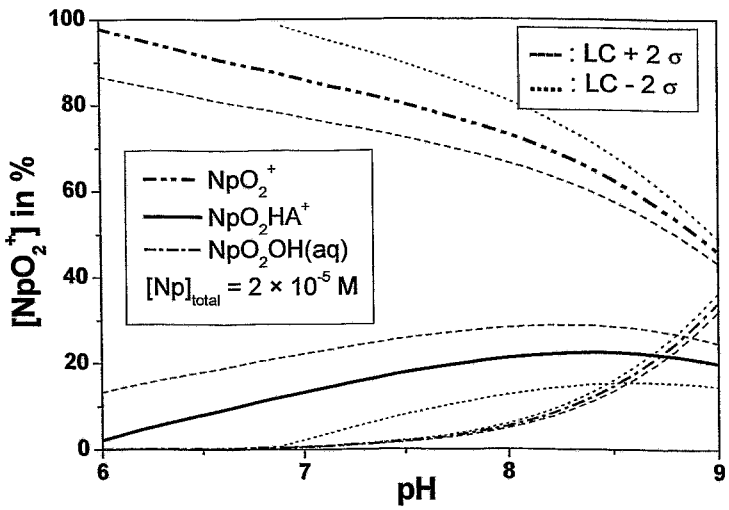

Fig. 8.2: Speciation of NpO_2^+ with HA as function of pH with uncertain LC values.

Similar results for U(VI) lead to the conclusions that a) the thermodynamic data sets for the interactions between actinides and HA are sparse and scattered, and b) LC as function of pH is not well defined, certainly caused by its very nature of being an empirical correction factor

subsuming many different effects. To obtain a more comprehensive picture of the situation a development of a respective database has been initiated.

There is no easy way to do speciation scans on varying pH like it can be done by members of the PHREEQE or MINEQL code families, not to talk from scans over varying Eh or the concentration of some components. To overcome this limitation at least partially, some tools have been written to allow such scans by automatically starting a sequence of EQ3NR runs with appropriately updated input files, or by analyzing and drastically shortening of the huge output from an EQ6 "titration" run. All these scripts can be found on the internet, the URL is:

http://www.fz_rossendorf.de/FWR/VB/EQ36/eq36.shtml

There is also a collection of tips and remarks for using EQ3/6 made available at:

http://www.fz_rossendorf.de/FWR/VB/EQ36/eq36_notes.shtml

Future research will focus on the separation of effects determining the LC value (namely protolysis reactions and aqueous metal ion speciation). It is also worth to investigate how to normalize properly the humic concentration with regard to the differently charged metal cations.

9 Development of a database for the application of the Metal Ion Charge Neutralization Model

Analyzing the data situation with regard to the Metal Ion Charge Neutralization Model (MICN) [11] it became clear that the data quality is very heterogeneous, values from different research groups are difficult to compare. For real complex natural systems a consistent database can hardly be compiled. The best solution would be to re-assess all existing experimental raw data for metal complexation with HA and process them consistently with respect to the MICN approach. However, due to limited resources a more realistic first step was to set-up (for the first time) a database covering all so far published reaction constants for the MICN model including the reported experimental conditions and data processing details. Such a database then provides an overview concerning investigated HA types, ligands, parameter ranges (concentration of reaction partners, ionic strength, pH, Eh, ...). The most critical gaps

can be identified and the data quality can be assessed more easily. At a later stage, also the automatic supply of data for speciation and reactive transport codes is possible.

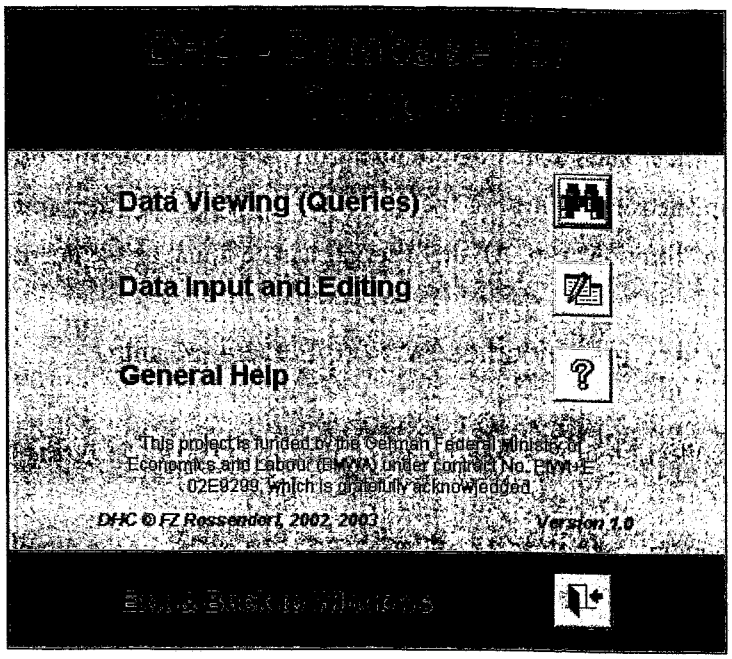

Fig. 9.1: Start menu of the humics complexation database DHC.

The "Database for Humics Complexation - DHC" is designed as a Relational Data Base System (**RDBS**), see Fig. 9.1 for the start menu. All information is structured into logical subunits, stored into separate tables which are logically connected by the RDBS. This ensures that every piece of information is only stored once. Other benefits are high efficiency with regard to storage capacity and access time, and internal consistency. In Fig. 9.2, a sketch of the major tables, their data elements, and their mutual relationships is given. The modular design also eases later extensions.

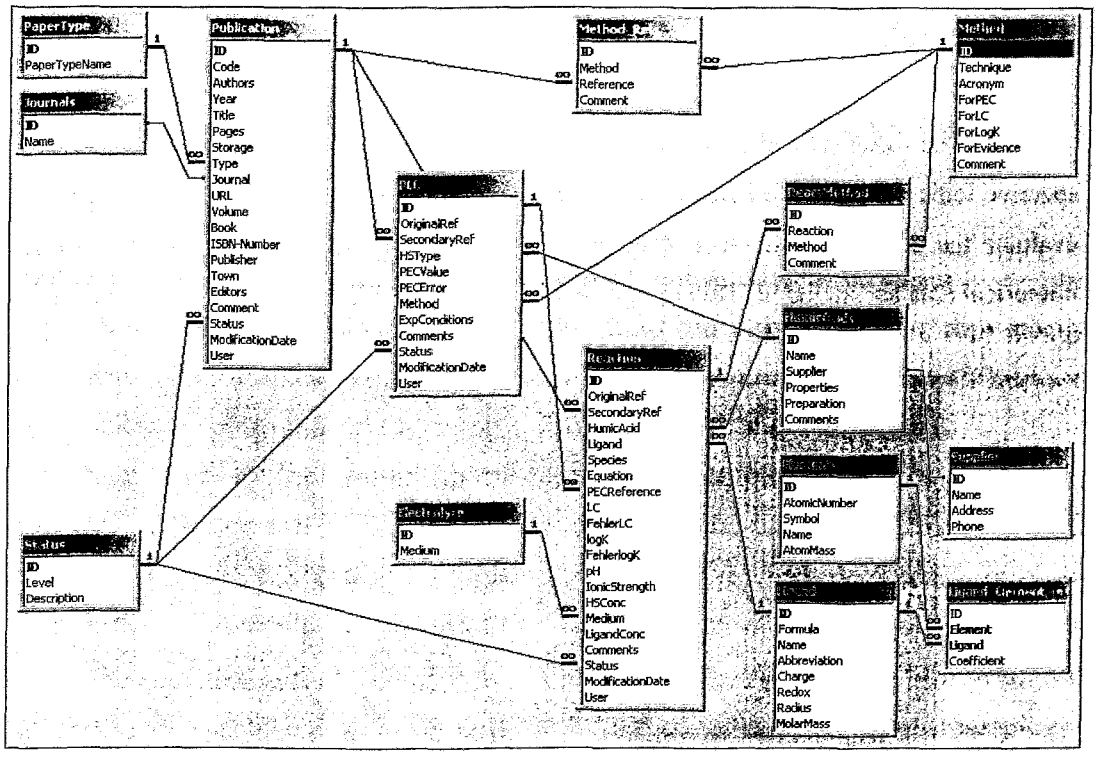

Fig. 9.2: Tables and their internal relations for the DHC RDBS.

The database is implemented in Microsoft Access on PC, providing an integrated graphical development system together with the RDBS. Data records can be displayed as tables, in forms or reports. Possible data types are: numeric, logic, text, binary object. Queries to the database can be performed with the standardized Structured Query Language (**SQL**), opening the opportunity to access external, additional databases, e.g. about spectroscopic data. Via SQL future versions of the DHC database can also be queried by web browsers. The programming of the database functionality can be enhanced by means of the Visual Basic for Application (**VBA**) programming language.

In general, all parameters recorded in the database are traced back to the original publication, including as many experimental details as possible to permit an evaluation of the data items. All internal relationships of complex data sets are stored, assuring a maximum of transparency and enabling the selection of internally consistent parameter sets. As an example, the input mask for the table containing complex formation constants is given in Fig. 9.3. Internal consistency means, that a complete data set for a HA and several aqueous complexing ligands (ions) is based upon the same values for the HA proton exchange capacity. In a strict sense,

even the pertinent aqueous speciation pattern in equilibrium with the surface complexes at the experimental conditions should be recorded, which is at the moment not implemented. For any value the experimental method used to derive this value is stored, together with the respective ionic strength and background media, as well as any other information necessary to evaluate the data or to calculate other derivative values. If published, uncertainty limits for numerical data are included. This is a prerequisite for sensitivity and uncertainty analysis.

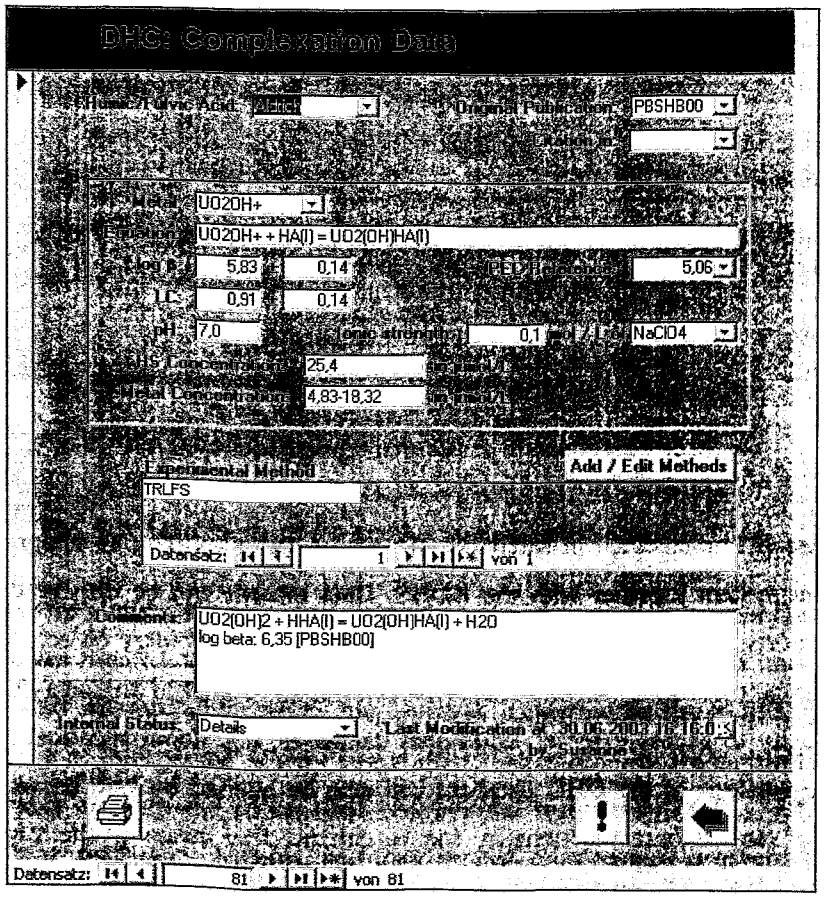

Fig. 9.3: Input mask in DHC for the loading capacity and complex formation data.

Instead of just being a (printed) collection of humics-meta complexation data, the approach presented here with a computer-based relational database opens additional opportunities of data processing by potential users via a graphical user interface.

In addition to such "hard" experimental results and parameters, an extensive bibliography is provided too. Every stored data item is linked to both original citations and secondary literature references. The references can also comprise model evaluations with respect to theoreti-

cal limitations, thermodynamic consistency and parameter sensitivity. Moreover, they cover questions of experimental design and interpretation of results from complexation experiments, or experimental methods used for such investigations with their associated error ranges and application areas.

The data records (each identified by a unique number) contain information about:

- Publication: abbreviation for citation, list of authors, year, title, pages, copy storage, type of publication, name of journal or book, volume, ISBN Number (if relevant), publisher, town, editor;
- Humic Acids: name, supplier (company or institute), properties, preparation;
- PEC: literature reference, citation, HA type, PEC value with associated error, experimental method, experimental conditions;
- Ligands: constituting elements, stoichiometry, charge, radius, redox state, molar mass;
- Method: name, abbreviation, check boxes for whether it can be applied to obtain values of PEC , LC or log β or if it is used for species identification / spectroscopic evidence;
- Reaction: literature reference, citation, HA type, ligand type, complex species, reaction equation, reference to PEC, LC with associated error, log β with associated error, pH, ionic strength, concentration of HA, background electrolyte type and concentration.

Besides, all major tables have a comment field, store the internal data record revision state, and keep the date and user name of the last editing.

The user interface allows several types of queries in addition to a mere scanning of the database content. Users can easily extract specific data sets, e.g. all records relevant for the combination of a specific HA and a specific ligand. They can also search for publications. Once a data set has been generated based on queries, it can be shown on the screen or printed out as a nicely formatted report. The results can also be exported into MS Excel spreadsheets for further processing.

As of November 2003, the DHC database covers 12 different types of HA, contains 20 data records for PEC and 81 complex formation constants with LC values. The data originate both from published papers and from research performed within the project.

The next step in the development of DHC will be the integration of an online manual. Based on a continuous extension and editing of the data content a systematic screening and data mining will help to reveal correlations and empirical internal dependencies of data. Provided enough resources can be allocated to the database, also the inclusion of the original experimental raw data is anticipated.

10 Summary and conclusions

In order to improve the knowledge on the interaction behavior of HA with metal ions HA model substances with specific functional properties were already developed at the Institute of Radiochemistry of the Forschungszentrum Rossendorf. Within this project a new batch of synthetic HA type M42 was synthesized and characterized. It was made available to all project partners thus enabling comparative model investigations. In addition to that, ^{14}C-labeled synthetic HA type M42 was synthesized. This radio-labeled HA model substance facilitates the precise determination of the fate of HA in sorption and migration experiments under environmentally relevant conditions.

From our former studies it is known that defined chemically modified HA are of great value for the study of the influence of specific HA functionalities on the interaction behavior of HA. In the present project a verified method for the synthesis of HA with blocked phenolic OH groups was optimized.

Within this project new HA model substances that are characterized by significantly more pronounced Fe(III) redox capacities than Aldrich HA were developed based on the oxidation of phenolic compounds. This synthetic HA help to improve the understanding of the effects of HA on the oxidation state of actinides.

Applying original and chemically modified synthetic HA with pronounced redox functionalities in comparison to natural HA from Aldrich and synthetic HA type M42 detailed studies on the redox properties of HA were performed. It was confirmed that HA phenolic/acidic OH groups play a significant role for the redox behavior of HA. However, the results show that there exist other processes than the single oxidation of phenolic OH groups and/or other HA functional groups that are also contributing to the redox properties of the studied substances.

The redox stability of U(VI) humate complexes of HA with distinct redox functionality was studied in comparison to Aldrich HA. Within these investigations the first direct spectroscopic proof for the reduction of U(VI) to U(IV) by the applied synthetic HA was succeeded.

The qualitative results indicate that the HA-like synthetic products show higher U(VI) redox capacities than Aldrich HA.

Structural and thermodynamical studies on the actinide complexation by HA applying synthetic HA model substances and natural HA were performed. It was focused on the determination of structural parameters for the interaction of HA with actinides in lower oxidation states (Pu(III), Th(IV), Np(IV) and Np(V)). The results indicate that the interaction between the actinide ions and HA is dominated by HA carboxylate groups. These carboxylate groups act predominantly as monodentate ligands.
Furthermore, we studied the influence of HA on the Np(V) complexation by HA in the neutral pH range in order to improve the understanding on functional groups contributing to the metal ion complexation by HA. The results obtained for Np(V) complexes with unmodified and chemically modified HA with blocked phenolic/acidic OH groups show that the complex formation is not influenced by phenolic/acidic OH groups with respect to the near-neighbor surrounding of Np(V) in its humate complexes (coordination numbers and bond lengths) and stability constants. However, the maximal available number of HA complexing sites decreases for HA with blocked phenolic groups.

Batch experiments were performed in order to determine the influence of HA on the Th(IV) sorption onto quartz and the Np(V) sorption onto granite and its mineral constituents. The influence of HA on the migration of U(IV)/(VI) in quartz was studied by means of column experiments. All sorption and migration experiments were performed applying ^{14}C-labeled synthetic HA type M42. It was found that Th(IV) and Np(V) show a pH dependent sorption behavior onto the studied materials which is affected by HA. In the case of the Np(V) sorption onto granite a slight decrease in the neptunium sorption is observed at pH values greater than pH 7 with addition of HA. Sorption studies with individual mineral components of granite show that biotite seems to be the mineral phase dominating the sorption in the studied system.
Humic acid M42 exhibits a significant influence on the transport of U(IV) and U(VI). In case of U(VI) a clear mobilizing effect was observed. There are strong indications for a similar influence of HA on the U(IV) transport. Both redox species of uranium differ slightly in their migration behavior in presence of HA. This is mainly reflected in a disagreement of their total recoveries.

The reliable geochemical modeling of the actinide transport requires the integration of the metal ion complexation with HA into existing geochemical speciation codes. Within this project the metal ion charge neutralization model was successfully embedded into the EQ3/6 geochemical speciation package. In addition to that, a verification of the changed EQ3/6 version was performed.

Before the present project no consistent data base on the HA metal ion complexation was available. Therefore, it was initiated to develop a respective data base. During the project a digital database was developed covering so far published HA complexation data based on the metal ion charge neutralization model.

The results of these studies improve the knowledge on the interaction of HA with actinides under aerobic and anaerobic conditions. Important results were obtained on the synthesis of specific HA model substances, the redox properties of HA, their complexation towards actinides and the influence of HA on the sorption and migration of actinides in lower oxidation states. A geochemical speciation code was enhanced and a new database developed. In their combination all results contribute to a more realistic description of the migration behavior of actinides in the environment and an improved risk assessment for instance for potential underground nuclear-waste repositories and former facilities of the uranium mining and milling.

Further studies should focus on the migration of actinides in the presence of HA in clay systems under aerobic and anaerobic conditions. In a first step kaolinite as model system for a clay environment should be investigated. In addition to that, further studies on the complexation of actinides, especially tetravalent, with HA have to be performed including kinetic processes and concurrent reactions with other metal ions. Further objectives are to continue the database for the HA metal ion complexation and to improve the metal ion charge neutralization model.

11 References

[1] Choppin, G.R.: Role of Humics in Actinide Behavior in Ecosystems. In: *Chemical Separation Technologies and Related Methods of Nuclear Waste Management* (Choppin, G.R., Khankhasayev, M. Kh., eds.). Kluwer Academic Publishers, 1999, p. 247-260.

[2] Abraham, A.: Einfluß von Huminstoffen und Holzabbauprodukten auf den Valenzzustand von Uran. PhD Thesis, TU Dresden, 2002.

[3] Kim, J.I.: Chemical Behaviour of Transuranic Elements in Natural Aquatic Systems. In: *Handbook on the Physics and Chemistry of the Actinides* (Freeman, A.J., Keller, C., eds.). Elsevier Science Publishers B.V., 1986, p. 413-455.

[4] Nash, K.L., Choppin, G.R.: Interaction of Humic and Fulvic Acids with Th(IV). J. Inorg. Chem. **42**, 1045 (1979).

[5] Li, W.C., Victor, D.M., Chakrabarti, C.L.: Effect of pH and Uranium Concentration on Interaction of Uranium(VI) and Uranium(IV) with Organic Ligands in Aqueous Solutions. Anal. Chem. **52**, 520 (1980).

[6] Choppin, G.R., Allard, B.: Complexes of Actinides with Naturally Occurring Organic Compounds. In: *Handbook on the Physics and Chemistry of the Actinides* (Freeman, A.J., Keller, C., eds.). Elsevier Science Publishers B.V., 1985, p. 407-429.

[7] Cacheris, W.P., Choppin, G.R.: Dissociation Kinetics of Thorium-Humate Complex. Radiochim. Acta **42**, 185 (1987).

[8] Moulin, V., Tits, J., Ouzounian, G.: Actinide Speciation in the Presence of Humic Acids in Natural Water Conditions. Radiochim. Acta **58/59**, 179 (1992).

[9] Rao, L.F., Choppin, G.R., Clark, S.B.: A Study of Metal-Humate Interactions using Cation Exchange. Radiochim. Acta **66/67**, 144 (1994).

[10] Pompe, S., Bubner, M., Schmeide, K., Heise, K.H., Bernhard, G., Nitsche, H.: Influence of Humic Acids on the Migration Behavior of Radioactive and Non-Radioactive Substances under Conditions Close to Nature. Synthesis, Radiometric Determination of Functional Groups, Complexation. Forschungszentrum Rossendorf, Wissenschaftlich-Technische Berichte, FZR-290, Rossendorf, Germany, 2000.

[11] Kim, J.I., Czerwinski, K.R.: Complexation of Metal Ions with Humic Acids: Metal Ion Charge Neutralization Model. Radiochim. Acta **73**, 5 (1996)

[12] Wolery, T.J.: EQ3/6, A Software Package for the Geochemical Modeling of Aqueous Systems. UCRL-MA-110662 Part 1, Lawrence Livermore National Laboratory, 1992.

[13] Kim, J.I., Buckau, G.: *Characterization of Reference and Site Specific Humic Acids.* RCM-Report 02188, TU München, 1988.

[14] Pompe, S.: Entwicklung huminsäureähnlicher Melanoidine als Funktionalitätsmodelle für Huminsäuren und ihr Vergleich mit Fluka-Huminsäure hinsichtlich ihres Komplexbildungsverhaltens gegenüber Uran(VI). PhD Thesis, TU Dresden, 1997.

[15] Pompe, S., Schmeide, K., Bubner, M., Geipel, G., Heise, K.H., Bernhard, G., Nitsche, H.: Investigation of Humic Acid Complexation Behavior with Uranyl Ions Using Modified Synthetic and Natural Humic Acids. Radiochim. Acta **88**, 553 (2000).

[16] Sachs, S., Bubner, M., Schmeide, K., Choppin, G.R., Heise, K.H., Bernhard, G.: Carbon-13 NMR Spectroscopic Studies on Chemically Modified and Unmodified Natural and Synthetic Humic Acids. Talanta **57**, 999 (2002).

[17] Bubner, M., Pompe, S., Meyer, M., Heise, K.H., Nitsche, H.: Isotopically Labelled Humic Acids for Heavy Metal Complexation. J. Labelled Cpd. Radiopharm. **XLI**, 1057 (1998).

[18] Stevenson, F.J.: *Humus Chemistry.* 2nd ed., John Wiley&Sons, New York, 1994.

[19] Stevenson, F.J.: *Humus Chemistry.* 1st ed., John Wiley&Sons, New York, 1982.

[20] Grauer, R.: Zur Koordinationschemie der Huminstoffe. Paul Scherrer Institut, Switzerland, Report No. 24, 1989, p. 7.

[21] Schnitzer, M., Khan, S.U.: *Humic Substances in the Environment* (A.D. McLaren, ed.). Marcel Dekker, Inc., New York, 1972.

[22] Bubner, M., Heise, K.H.: Characterization of Humic Acids. II. Characterization by Radioreagent-Derivatization with [^{14}C]Diazomethane. In: *FZR-43, Annual Report 1993* (Nitsche, H., Bernhard, G., eds.), Forschungszentrum Rossendorf, Institute of Radiochemistry, Rossendorf, Germany, 1994, p. 22.

[23] Schmeide, K., Sachs, S., Bubner, M., Reich, T., Heise, K.H., Bernhard, G.: Interaction of Uranium(VI) with Various Modified and Unmodified Natural and Synthetic Humic Substances Studied by EXAFS and FTIR Spectroscopy. Inorg. Chim. Acta **351**, 133 (2003).

[24] Baraniak, L., Mack, B., Abraham, A., Neubert, H.: Abschlußbericht zum Forschungsvorhaben "Untersuchung des Einflusses der in Grubenwässern gelösten organischen Verbindungen auf den Valenzzustand von Radionukliden und Schwermetallen im Hinblick auf den Flutungsprozeß der sächsischen Uranbergwerke". Förderkennzeichen: 4-7541.83-FZR/512. Forschungszentrum Rossendorf 1997.

[25] Beyer, H., Walter, W.: Lehrbuch der organischen Chemie. S. Hirzel Verlag, Stuttgart, 22nd ed., 1991.

[26] Eller, W., Koch, K.: Synthetische Darstellung von Huminsäuren. Berichte Dt. Chem. Gesellschaft **53**, 1469 (1920).

[27] Adhikari, M., Sen, P., Krishnendu, D.: Studies on Synthesis of Humic Substances in Laboratory under Different Conditions. Proc. Indian Natn. Sci. Acad. **51A**, 876 (1985).

[28] Mack, B., Baraniak, L., Heise, K.H., Bernhard, G., Nitsche, H.: Reduction of Iron(III) by Natural and Synthetic Melanoidine-Type Humic Acids. In: *FZR-285, Annual Report 1999*

(Bernhard, G., ed.), Forschungszentrum Rossendorf, Institute of Radiochemistry, Rossendorf, Germany, 2000, p. 40.

[29] Mack, B.: Redoxeigenschaften von Lignin und Huminsäuren und deren Wechselwirkung mit Eisen. PhD Thesis, TU Dresden, 2002.

[30] Standard Methods for the Examination of Water and Wastewater (Greenberg, A.E., Clesceri, L.S., Eaton, A.D., eds.). American Public Health Association, 18th ed., Washington DC, 1992.

[31] Matthiessen, A.: Determining the Redox Capacity of Humic Substances as a Function of pH. Vom Wasser **84**, 229 (1995).

[32] Stewart, R. : *Oxidation Mechanisms. Applications to Organic Chemistry.* W.A. Benjamin, Inc., New York, 1964, ch. 3.

[33] Mc Donald, P.D., Hamilton, G.A.: Mechanisms of Phenolic Oxidative Coupling Reactions. In: *Oxidation in Organic Chemistry* (Trahanovsky, W.S., ed.). Academic Press, New York, 1973, ch. 2.

[34] Helburn, R.S., MacCarthy, P.: Determination of Some Redox Properties of Humic Acid by Alkaline Ferricyanide Titration. Anal. Chim. Acta **25**, 263 (1994).

[35] Geipel, G., Bernhard, G., Brendler, V., Nitsche, H.: Complex Formation between UO_2^{2+} and CO_3^{2-}: Studied by Laser-Induced Photoacoustic Spectroscopy (LIPAS). Radiochim. Acta **82**, 59 (1998).

[36] Geipel, G., Bernhard, G., Brendler, V.: Complex Formation of Uranium(IV) with Phosphate and Arsenate. In: *Uranium in the Aquatic Environment* (Merkel, B.J., Planer-Friedrich, B., Wolkersdorfer, C., eds.). Springer Verlag, Berlin, 2002, p. 369-376.

[37] Koningsberger, D.C., Prins, R. (eds.): *X-ray Absorption: Principles, Applications, Techniques of EXAFS, SEXAFS and XANES.* Wiley, New York, USA, 1988.

[38] Schmeide, K., Zänker, H., Heise, K.H., Nitsche, H.: Isolation and Characterization of Aquatic Humic Substances from the Bog 'Kleiner Kranichsee'. In: *FZKA 6124, Wissenschaftliche Berichte* (Buckau, G., ed.), Forschungszentrum Karlsruhe, Karlsruhe, Germany, 1998, p. 161-195.

[39] Pompe, S., Bubner, M., Denecke, M.A., Reich, T., Brachmann, A., Geipel, G., Nicolai, R., Heise, K.H., Nitsche, H.: A Comparison of Natural Humic Acids with Synthetic Humic Acid Model Substances: Characterization and Interaction with Uranium(VI). Radiochim. Acta **74**, 135 (1996).

[40] Schmeide, K., Sachs, S., Reich, T., Brendler, V., Heise, K.H., Bernhard, G.: Neptunium(IV) Complexation by Humic Substances Studied by X-ray Absorption Fine Structure Spectroscopy. Radiochim. Acta, submitted.

[41] Schmeide, K., Sachs, S., Reich, T., Heise, K.H., Bernhard, G.: Plutonium(III) Complexation by Humic Substances Studied by X-ray Absorption Fine Structure Spectroscopy, in preparation.

[42] Sachs, S., Schmeide, K., Reich, T., Brendler, V., Heise, K.H., Bernhard, G.: EXAFS Study on the Neptunium(V) Complexation by Various Humic Acids under Neutral Conditions. Radiochim. Acta, submitted.

[43] Reich, T., Bernhard, G., Geipel, G., Funke, H., Hennig, C., Roßberg, A., Matz, W., Schell, N., Nitsche, H.: The Rossendorf Beam Line ROBL – A Dedicated Experimental Station for XAFS Measurements of Actinides. Radiochim. Acta **88**, 633 (2000).

[44] George, G.N., Pickering, I.J.: *EXAFSPAK: A Suite of Computer Programs for Analysis of X-Ray Absorption Spectra*. Stanford Synchrotron Radiation Laboratory, Stanford, USA, 1995.

[45] Zabinsky, S.I., Rehr, J.J., Ankudinov, A., Albers, R.C., Eller, M.J.: Multiple Scattering Calculations of X-ray Absorption Spectra. Phys. Rev. B, **52**, 2995 (1995).

[46] Denecke, M.A., Bublitz, D., Kim, J.I., Moll, H., Farkes, I.: EXAFS Investigation of the Interaction of Hafnium and Thorium with Humic Acid and Bio-Rex70. J. Synchrotron Rad. **6**, 394 (1999).

[47] Moll, H., Denecke, M.A., Jalilehvand, F., Sandström, M., Grenthe, I.: Structure of the Aqua Ions and Fluoride Complexes of Uranium(IV) and Thorium(IV) in Aqueous Solution an EXAFS Study. Inorg. Chem. **38**, 1795 (1999).

[48] Zhang, Y.-J., Collison, D., Livens, F.R., Powell, A.K., Wocadlo, S., Eccles, H.: Synthesis, Spectroscopic, and X-ray Crystallographic Characterization of Thorium(IV) and Uranium(IV) Malonato and Substituted Malonato Compounds. Polyhedron **19**, 1757 (2000).

[49] Akhtar, M.N., Smith, A.J.: The Crystal Structure of Tetrapotassium Tetraoxalatothorium(IV) Tetrahydrate, $K_4Th(C_2O_4)_4 \cdot 4H_2O$. Acta Crystallogr. **B31**, 1361 (1975).

[50] Antonio, M.R., Soderholm, L., Williams, C.W., Blaudeau, J.-P., Bursten, B.E.: Neptunium Redox Speciation. Radiochim. Acta **89**, 17 (2001).

[51] Allen, P.G., Bucher, J.J., Shuh, D.K., Edelstein, N.M., Reich, T.: Investigation of Aquo and Chloro Complexes of UO_2^{2+}, NpO_2^{+}, Np^{4+}, and Pu^{3+} by X-ray Absorption Fine Structure Spectroscopy. Inorg. Chem. **36**, 4676 (1997).

[52] Denecke, M.A., Pompe, S., Reich, T., Moll, H., Bubner, M., Heise, K.H., Nicolai, R., Nitsche, H.: Measurements of the Structural Parameters for the Interaction of Uranium(VI) with Natural and Synthetic Humic Acids using EXAFS. Radiochim. Acta **79**, 151 (1997).

[53] Denecke, M.A., Reich, T., Pompe, S., Bubner, M., Heise, K.H., Nitsche, H., Allen, P.G., Bucher, J.J., Edelstein, N.M., Shuh, D.K., Czerwinski, K.R.: EXAFS Investigations on the Interaction of Humic Acids and Model Compounds with Uranyl Cations in Solid Complexes. Radiochim. Acta **82**, 103 (1998).

[54] Grigoriev, M.S., Charushnikova, I.A., Krot, N.N., Yanovskii, A.I., Struchkov, Yu.T.: Crystal Structure of Neptunium(IV) Oxalate Hexahydrate $Np(C_2O_4)_2 \cdot 6H_2O$. Radiokhim. **39**, 419 (1997).

[55] Hauck, J.: The Crystal Structure of $Me(HCOO)_4$, Me = Th, Pa, U, Np. Inorg. Nucl. Chem. Lett. **12**, 617 (1976).

[56] Neck, V., Kim, J.I.: An Electrostatic Approach for the Prediction of Actinide Complexation Constants with Inorganic Ligands-Application to Carbonate Complexes. Radiochim. Acta **88**, 815 (2000).

[57] Grigoriev, M.S., Charushnikova, I.A., Krot, N.N., Yanovskii, A.I., Struchkov, Yu.T.: Crystal and Molecular Structure of Neptunyl Malonate Tetrahydrate $(NpO_2)_2C_3H_2O_4 \cdot 4H_2O$. Radiokhim. **4**, 24 (1993).

[58] Grigoriev, M.S., Charushnikova, I.A., Krot, N.N., Yanovskii, A.I., Struchkov, Yu.T.: Crystal Structure of the Neptunyl Formate Complex $(NH_4)NpO_2(OOCH)_2$. J. Neorgan. Chim. **39**, 1328 (1994).

[59] Reich, T., Geipel, G., Funke, H., Hennig, C., Roßberg, A., Bernhard, G.: First XANES and EXAFS Measurements of Plutonium Solutions at ROBL. In: *FZR-285, Annual Report 1999* (Bernhard, G., ed.). Forschungszentrum Rossendorf, Institute of Radiochemistry, Rossendorf, Germany, 2000, p. 72.

[60] Ankudinov, A.L., Conradson, S.D., Mustre de Leon, J., Rehr, J.J.: Relativistic XANES Calculations of Pu Hydrates. Phys. Rev. **B57**, 7518 (1998).

[61] Lemire, R.J., Fuger, J., Nitsche, H., Potter, P., Rand, M.H., Rydberg, J., Saphiu, K., Sullivan, J.C., Ullman, W.J., Vitorge, P., Wanner H.: *Chemical Thermodynamics of Neptunium and Plutonium.* Elsevier Science B.V., Amsterdam, 2001.

[62] Kim, J.I., Sekine, T.: Complexation of Neptunium(V) with Humic Acid. Radiochim. Acta **55**, 187 (1991).

[63] Marquardt, C., Kim, J.I.: Complexation of Np(V) with Humic Acid: Intercomparison of Results from Different Laboratories. **80**, 129 (1998).

[64] Seibert, A., Mansel, A., Marquardt, C.M., Keller, H., Kratz, J.V., Trautmann, N.: Complexation Behaviour of Neptunium with Humic Acid. Radiochim. Acta **89**, 505 (2001).

[65] Schild, D., Marquardt, C.M.: Analysis of Th(IV)-humate by XPS. Radiochim. Acta **88**, 587 (2000).

[66] Davis, J.R., Higgo, J.J.W., Noy, D.J., Hooker, P.J.: Complexation Studies of Uranium and Thorium with Natural Fulvic Acid. In: *FZKA 6524, Wissenschaftliche Berichte* (Buckau, G., ed.), Forschungszentrum Karlsruhe, Karlsruhe, Germany, 2000, p. 87-99.

[67] Reiller, P., Moulin, V., Dautel, Ch., Casanova, F.: Complexation of Th(IV) by Humic Substances. In: *FZKA 6524, Wissenschaftliche Berichte* (Buckau, G., ed.), Forschungszentrum Karlsruhe, Karlsruhe, Germany, 2000, p. 121-129.

[68] Östhols, E., Manceau, A., Farges, F., Charlet, L. : Adsorption of Thorium on Amorphous Silica : An EXAFS Study. J. Coll. Interf. Sci. **194**, 10 (1997).

[69] Murphy, R.J., Lenhart, J.J., Honeyman, B.D.: The Sorption of Thorium(IV) and Uranium(VI) to Hematite in the Presence of Natural Organic Matter. Colloids and Surfaces. A: Physical and Engineering Aspects **157**, 47 (1997).

[70] Reiller, P., Moulin, V., Dautel, Ch.: Sorption Behavior of Humic Substances towards Hematite : Consequences on Thorium Availability. In: *FZKA 6524, Wissenschaftliche Berichte* (Buckau, G., ed.), Forschungszentrum Karlsruhe, Karlsruhe, Germany, 2000, p. 133-147.

[71] Reiller, P., Moulin, V., Dautel, Ch.: Complexation of Eu(III), Th(IV), and U(VI) by Humic Substances. In: *FZKA 6324, Wissenschaftliche Berichte* (Buckau, G., ed.), Forschungszentrum Karlsruhe, Karlsruhe, Germany, 1999, p. 82-117.

[72] Reiller, P., Moulin, V., Casanova, F., Dautel, Ch.: On the Study of Th(IV)-Humic Acid Interactions by Competition Sorption Studies with Silica and Determination of Global Interaction Constants. Radiochim. Acta **91**, 513 (2003).

[73] Stumm, W.: *Chemistry of the Solid-Water Interface, Processes at the Mineral-Water and Particle-Water Interface in Natural Systems.* John Wiley & Sons, Inc., 1992.

[74] Papp, R.: Gegenüberstellung von Endlagerkonzepten in Salz und Hartgestein. FZKA-PTE Nr. 3, Forschungszentrum Karlsruhe GmbH, Karlsruhe 1997.

[75] Krawczyk-Bärsch, E., Arnold, T., Bernhard, G.: Das Sorptionsverhalten von U(VI) am Granit von Eibenstock (Erzgebirge) und seinen mineralogischen Komponenten. European Journal of Mineralogy **13**, 103 (2001).

[76] Arnold, T., Forschungszentrum Rossendorf, personal communication.

[77] Nakata, K., Nagasaki, S., Tanaka, S., Sakamoto, Y., Tanaka, T., Ogawa, H.: Sorption and Reduction of Neptunium(V) on the Surface of Iron Oxides. Radiochim. Acta **90**, 665 (2002).

[78] Zeh, P., Kim, J.I., Marquardt, C.M., Artinger, R.: The Reduction of Np(V) in Groundwater Rich in Humic Substances. Radiochim. Acta **87**, 23 (1999).

[79] Kim, J.I., Delakowitz, B., Zeh, P., Klotz, D., Lazik, D.: A Column Experiment for the Study of Colloidal Radionuclide Migration in Gorleben Aquifer Systems. Radiochim. Acta **66/67**, 165 (1994).

[80] Artinger, R., Rabung, T., Kim, J.I., Sachs, S., Schmeide, K., Heise, K.H., Bernhard, G., Nitsche, H.: Humic Colloid-borne Migration of Uranium in Sand Columns. J. Contam. Hydr. **58**, 1 (2002).

[81] Artinger, R., Kienzler, B., Schuessler, W., Kim, J.I.: Effects of Humic Substances on the ^{241}Am Migration in a Sandy Aquifer: Batch and Column Experiments with Gorleben Groundwater/Sediment Systems. J. Contam. Hydr. **35**, 261 (1998).

[82] Artinger, R., Seibert, A., Marquardt, C.M., Trautmann, N., Kratz, J.V., Kim, J.I.: Humic Colloid-borne Np Migration: Influence of the Oxidation State. Radiochim. Acta **88**, 609 (2000).

[83] Pompe, S., Brachmann, A., Bubner, M., Geipel, G., Heise, K.H., Bernhard, G., Nitsche, H.: Determination and Comparison of Uranyl Complexation Constants with Natural and Model Humic Acids, Radiochim. Acta **82**, 89 (1998).

[84] Bertrand, P.A., Choppin, G.R.: Separation of Actinides in Different Oxidation States by Solvent Extraction. Radiochim. Acta **31**, 135 (1982).

[85] Toride, N., Leji, F.J., van Genuchten, M.Th.: The CXTFIT Code for Estimating Transport Parameters from Laboratory or Field Tracer Experiments. Version 2.1. Research Report No. 137. U.S. Salinity Laboratory, Agricultural Research Service, U.S. Department of Agriculture, Riverside, California (1995).

[86] Grolimund, D., Elimelech, M., Borkovec, M., Barmettler, K., Kretzschmar, R., Sticher, H.: Transport of in Situ Mobilized Colloidal Particles in Packed Soil Columns. Environ. Sci. Technol. **32**, 3562 (1998).

[87] Grenthe, I., Fuger, J., Konings, R.J.M., Lemire, R.J., Muller, A.B., Nguyen-Trung, C., Wanner, H.: *Chemical Thermodynamics, Volume 1: Chemical Thermodynamics of Uranium.* North-Holland, Amsterdam, 1992.

[88] Choppin, G.R.: Solution Chemistry of the Actinides. Radiochim. Acta **32**, 43 (1983).

[89] Tipping, E.: Humic Ion-Binding Model VI: An Improved Description of the Interactions of Protons and Metal Ions with Humic Substances. Aquatic Geochem. **4**, 3 (1998).

[90] Torres, R.A., Choppin, G.R.: Europium(III) and Americium(III) Stability Constants with Humic Acid. Radiochim. Acta **35**, 143 (1984).

[91] Kinniburgh, D.G., Milne, C.J., Benedetti, M.F., Pinheiro, J.P., Filius, J., Koopal, L.K., Van Riemsdijk, W.H.: Metal Ion Binding by Humic Acid: Application of the NICA-Donnan Model. Environ. Sci. Technol. **30**, 1687 (1996).

[92] Van Riemsdijk, W.H., de Wit, J.C.M., Mous, S.L.J., Koopal, L.K., Kinniburgh, D.G.: An Analytical Isotherm Equation (CONICA) for Nonideal Mono and Bidentate Competitive Ion Adsorption to Heterogeneous Surfaces. J. Colloid Interface Sci. **183**, 35 (1996).

12 Acknowledgement

The authors would like to thank M. Meyer and R. Ruske for their valuable help in synthesizing and characterization of HA and their technical assistance. Thanks are given to H. Foerstendorf, R. Nicolai and K. Muschter for FTIR measurements and H. Görner for elemental analysis. We thank U. Schaefer for ICP-MS measurements.

EXAFS measurements were performed at BM20 at the European Synchrotron Radiation Facility in Grenoble (France). In particular, thanks are given to T. Reich, C. Hennig, H. Funke, A. Roßberg and H. Moll for their support during EXAFS measurements and the evaluation of the EXAFS data. We thank G. Grambole for her help in preparation and characterization of EXAFS samples.

Thanks are given to B. Barz and R. Jander for their help in the performance of batch experiments. We thank J. Tutschku for the electrochemical reduction of uranium(VI) and S. Brockmann for their technical assistance during the column experiments. The authors thank C. Nebelung for the evaluation of LSC spectra.

At this place we would like to thank all colleagues who contributed to the success of this work.